Cardiovascular mathematics

Alfio Quarteroni*

Abstract. In this paper we introduce some basic differential models for the description of blood flow in the circulatory system. We comment on their mathematical properties, their meaningfulness and their limitation to yield realistic and accurate numerical simulations, and their contribution for a better understanding of cardiovascular physio-pathology.

Mathematics Subject Classification (2000). 92C50,96C10,76Z05,74F10,65N30,65M60.

Keywords. Cardiovascular mathematics; mathematical modeling; fluid dynamics; Navier–Stokes equations; numerical approximation; finite element method; differential equations.

1. Introduction

The cardiovascular system has the task of supplying the human organs with blood. Its main components are the heart, the arteries and the veins. The so-called *large* (systemic) *circulation* brings oxygenated blood from the left ventricle via the aorta to the various organs through the arterial system, then brings it back through the venous system and the vena cava to the right atrium.

The *small circulation* is the one between the heart and the lungs. Blood is pumped from the right ventricle via the pulmonary artery to the lungs at a peak pressure of about 4 kPa. Venous blood enters the pulmonary system, gets oxygenated and returns to the left heart atrium (see Figure 1). In the past decade, the application of mathematical models, seconded by the use of efficient and accurate numerical algorithms, has made impressive progress in the interpretation of the circulatory system functionality, in both physiological and pathological situations, as well as in the perspective of providing patient specific design indications to surgical planning.

This has called for the development of a new field of applied mathematics: however, although many substantial achievements have been made in the field of modeling, mathematical and numerical analysis, and scientific computation, where a variety of new concepts and mathematical techniques have been introduced, most of the difficulties are still on the ground and represent major challenges for the years to come.

*I gratefully acknowledge the help from L. Formaggia, A. Veneziani, P. Zunino (MOX-Politecnico di Milano), G. Fourestey, G. Rozza (CMCS-EPFL) during the preparation of these notes. This research has been made possible by the financial support of EU Project HPRN-CT-2002-00270 "Haemodel", the MIUR grant "Numerical Modelling for Scientific Computing and Advanced Applications" and the INDAM grant "Integration of Complex Systems in Biomedicine".

Proceedings of the International Congress
of Mathematicians, Madrid, Spain, 2006

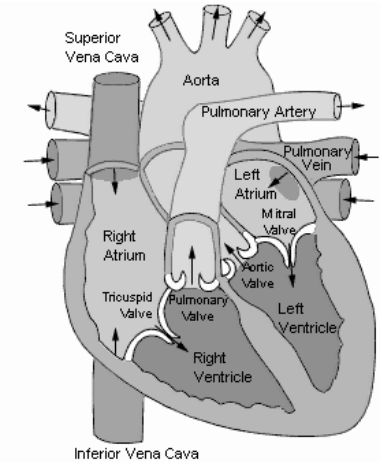

Figure 1. The human heart. Courtesy of the Texas Heart®Institute.

The main impulse to develop this field of study is the increasing demand from the medical community for scientifically rigorous and quantitative investigations of cardiovascular diseases, which are responsible today for about the 40% od deaths in industrialized societies. The 3/4 of them are related to atherosclerosis, which manifests as, e.g., stroke, myocardial infarction or peripheral vascular diseases. For example, in vascular surgery, arterial bypass grafting is a common practice to treat coronary artery and peripheral vascular diseases. Nonetheless, over 50% of coronary artery bypass grafts fail within 10 years and more than 25% of infra-inguinal grafts within 5 years (see [9], [31], [96]). The principal cause is neo-intimal hyperplasia that may degenerate in atherosclerosis. A better understanding of local haemodynamics, like the detection of regions of low wall shear stress and of high residence time for blood particles, is of utmost importance to assess its correlation with atherogenesis ([11]).

The vascular system is highly complex and able to regulate itself: an excessive decrease in blood pressure will cause the smaller arteries (the arterioles) to contract and the heart rate to increase, whereas an excessive blood pressure is counter-reacted by a relaxation of the arterioles (which causes a reduction of the periphery resistance to the flow) and a decrease of the heart beat. Yet, it may happen that some pathological conditions develop. For example, the arterial wall may become more rigid, due to illness or excessive smoking habits, fat may accumulate in the arterial walls causing a reduction of the vessel section (a stenosis) and eventually an aneurysm may develop. The consequence of these pathologies on the blood field as well as the possible outcome of a surgical intervention to cure them may be studied by numerical simulations, that are less invasive than *in-vivo* investigation, and far more accurate and flexible than *in-vitro* experiments. Numerical models require patient's data (the

initial and boundary conditions for the PDE systems, as well as geometrical data to characterize the shape of the computational domain) that can be generated by radiological acquisition through, e.g., computer tomography, magnetic resonance, doppler anemometry, etc. Besides their employment in medical research, numerical models of vascular flows can provide a virtual experimental platform to be used as training system. For instance, a technique now currently used to cure a stenosis is angioplasty, which consists of inflating a balloon positioned in the stenotic region by the help of a catheter. The balloon should squash the stenosis and approximately restore the original lumen area. The success of the procedure depends, among other factors, on the sensitivity of the surgeon and his ability of placing the catheter in the right position. A training system which couples virtual reality techniques with the simulation of the flow field around the catheter, the balloon and the vessel walls, employing geometries extracted from real patients, could well serve as training bed for new vascular surgeons. A similar perspective could provide specific design indications for the realization of surgical operations. For instance, numerical simulations could represent a tool for the design of new prototypes, or for devising prosthetic devices by the help of shape optimization theory. In particular, shape optimization has been used for minimizing the downstream vorticity in coronary by-pass grafts (see [1], [76], [85]). These numerical investigations can help the surgeon in understanding how the different surgical solutions may affect blood circulation and guide the choice of the most appropriate procedure for a specific patient. In such "virtual surgery" environments, the outcome of alternative treatment plans for the individual patient can be foreseen by simulations, yielding a new paradigm of the clinical practice which is referred to as "predictive medicine" (see [92]).

In this presentation we will address some of the most basic models that are used to describe blood flow dynamics in local arterial environments (Section 2) and to predict the vessel wall deformation in compliant arteries (Section 3). Then we will introduce appropriate geometrical multiscale models that integrate three-dimensional, one-dimensional and zero-dimensional models for the simulation of blood circulation in the whole arterial tree (Section 4). Finally, in Section 5 we consider the problem of modeling biochemical processes occurring across the several layers of the arterial wall.

2. Mathematical models for local blood flow dynamics

The mathematical equations of fluid dynamics are the key components of haemodynamics modeling. Rigorously speaking, blood is not a fluid but a suspension of particles in a fluid called *plasma*, which is made of water for the 90–92%, proteins (like serum albumin, globulins and fibrinogen) for the 7% and inorganic constituents for the rest. The most important blood particles are red cells, white cells and platelets. Red cells (erythrocytes) are responsible for the exchange of oxygen and carbon-dioxide with the cells. They are about $4\text{–}6 \cdot 10^6$ biconcave disks per mm^3 and provide the

45% of blood volume; they are made by the 65% of water, the 3% of membrane components, and around the 32% by haemoglobin.

White cells (leukocytes), play a major role in the human immune system: they are (roughly) spherical, and are $4–11 \cdot 10^3$ per mm^3. Platelets (thrombocytes) are the main responsible for blood coagulation: they are rounded or oval disks and there are $3–5 \cdot 10^5$ per mm^3.

Rheological models in smaller arterioles and capillaries should account for the presence of blood cells since their size becomes comparable to that of the vessel. In this section, however, we will bound our investigation to flow in *large and medium sized vessels*.

The principal quantities which describe blood flow are the *velocity* $\boldsymbol{u}$ and *pressure* P. Knowing these fields allows the computation of the *stresses* to which an arterial wall is subjected due to the blood movement. When addressing fluid-structure interaction problems (see Section 3), the *displacement* of the vessel wall due to the action of the flow field is another quantity of relevance. Pressure, velocity and vessel wall displacement will be functions of time and the spatial position. Accounting for *temperature* variation may be relevant in some particular context, for instance in the hyperthermia treatment, where some drugs are activated through an artificial localized increase in temperature (see [47], [28]). Temperature may also have a notable influence on blood properties, in particular on blood viscosity. Yet, this aspect is relevant only in the flow through very small arterioles/veins and in the capillaries, a subject which is covered only partially in these notes. Another aspect related with blood flow modeling is the *chemical interaction* with the vessel wall, which is relevant both for the physiology of the blood vessels and for the development of certain vascular diseases. Not mentioning the potential relevance of such investigation for the study of the propagation/absorption of pharmaceutical chemicals. A short account will be given in Section 5.

A major feature of blood flow is represented by its pulsatility. With some approximation one may think the blood flow to be periodic in time. Yet, this is usually true only for relatively short periods, since the various human activities require to change the amount of blood sent to the various organs. The cardiac cycle features two distinct phases. The *systolic* phase, when the heart pumps the blood into the arterial system, is characterized by the highest flow rate. The *diastolic* phase is when the heart is filling up with the blood coming from the venous system and the aortic valve is closed. Figure 2 illustrates a typical flow rate curve of a large artery during the cardiac cycle. Pulsatility induces flow reversal which manifests near arterial walls, a phenomenon that can enhance the appearance of stenoses in specific vascular districts, like the carotid bifurcation (see Figure 3).

To simplify our presentation, in this section we will introduce the flow equations in a "truncated" blood vessel like the one illustrated in Figure 4, which is representative of a small portion of the arterial system. We will make the further assumption that the vessel is rigid, thus the flow domain, denoted by Ω, is independent of time. (This unphysical restriction will be removed in next section where we will specifically

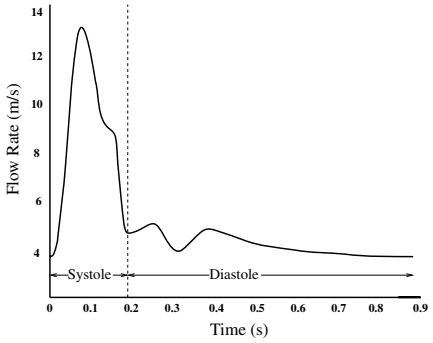

Figure 2. A typical flow rate in an artery during the cardiac cycle.

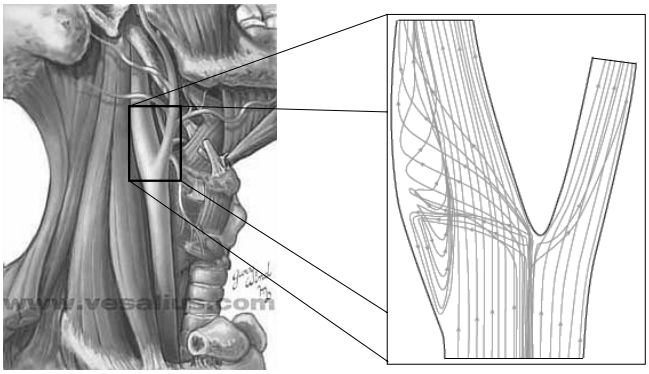

Figure 3. Recirculation in the carotid bifurcation. On the left we illustrate the location of the carotid bifurcation. The image on the right shows the particle path during the diastolic period in a model of the carotid bifurcation. A strong recirculation occurs inside the carotid sinus. The image on the left is courtesy of vesalius.com.

address the interaction between blood flow and arterial wall deformation.) If we denote by $\rho = \rho(\boldsymbol{x}, t)$ the blood density and by $\boldsymbol{u} = \boldsymbol{u}(\boldsymbol{x}, t)$ the blood velocity, the principle of conservation of mass yields the *continuity equation*

$$\partial_t \rho + \operatorname{div}(\rho \boldsymbol{u}) = 0 \quad \text{for } x \in \Omega,\ t > 0 \tag{1}$$

where ∂_t is the partial derivative w.r.t. t, while $\operatorname{div} \boldsymbol{u} = \sum_{i=1}^{3} \partial_{x_i} u_i$ is the spatial divergence of the vector field $\boldsymbol{u}$.

In large and medium size vessels the blood density can be assumed to be constant, then from (1) we derive the kinematic constraint

$$\operatorname{div}(\boldsymbol{u}) = 0 \quad \text{in } \Omega, \tag{2}$$

which in view of the Euler expansion formula implies flow incompressibility.

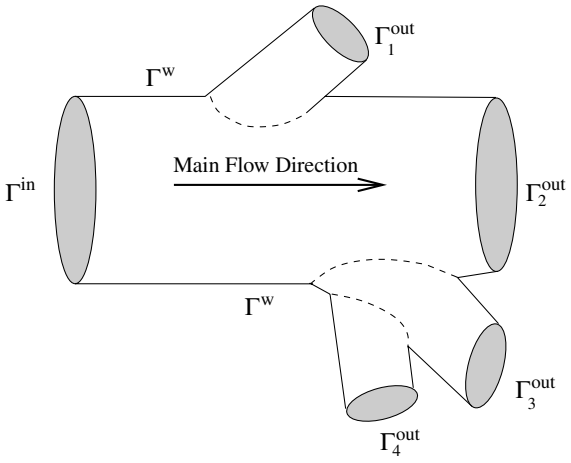

Figure 4. An example of a computational domain made of a section of the vascular system. We need to provide proper boundary conditions at inflow Γ^{in}, outflow Γ^{out} and wall Γ^{w}.

On the other hand, the principle of conservation of momentum, which states that body forces, applied surface forces and internal "cohesion" forces must be in equilibrium, writes

$$\rho \frac{D\boldsymbol{u}}{Dt} - \operatorname{div}(\boldsymbol{T}) = \rho \boldsymbol{f} \quad \text{for } x \in \Omega,\ t > 0, \tag{3}$$

where $\frac{D\boldsymbol{u}}{Dt} = \partial_t \boldsymbol{u} + (\boldsymbol{u} \cdot \nabla)\boldsymbol{u}$ is the fluid acceleration (∇ is the spatial gradient), $\boldsymbol{f}$ is the specific body force (e.g., $\boldsymbol{f} = -g\boldsymbol{e_3}$ where $\boldsymbol{e_3}$ represents the unit vector in the vertical direction and g the gravitational acceleration), while $\boldsymbol{T}$ is the Cauchy stress tensor (see [3] and [86]). The system (2),(3) can be closed by using a constitutive law that relates the Cauchy stress to kinematic quantities (velocity and pressure), and which is peculiar to the specific rheological behavior of the fluid under consideration. In large and medium size vessel, blood behaves as a Newtonian incompressible fluid, where we have

$$\boldsymbol{T} = -P\boldsymbol{I} + 2\mu \boldsymbol{D}(\boldsymbol{u}); \tag{4}$$

P is a scalar function (the pressure), $\boldsymbol{I}$ is the identity matrix, μ is the dynamic viscosity, $\boldsymbol{D}(\boldsymbol{u}) = \frac{1}{2}(\nabla \boldsymbol{u} + \nabla \boldsymbol{u}^T)$ is the *strain rate* tensor, $D_{ij} = \frac{1}{2}\big(\frac{\partial u_i}{\partial x_j} + \frac{\partial u_j}{\partial x_i}\big)$, $i, j = 1, \ldots, 3$. Then (3) becomes

$$\partial_t \boldsymbol{u} + (\boldsymbol{u} \cdot \nabla)\boldsymbol{u} + \nabla p - 2\operatorname{div}(\nu \boldsymbol{D}(\boldsymbol{u})) = \boldsymbol{f} \tag{5}$$

where $p = \frac{P}{\rho}$ is a scaled pressure and $\nu = \frac{\mu}{\rho}$ is the kinematic viscosity. More in general, ν may depend on kinematic quantities. Several models have been proposed in this respect, as we will see later in this section.

The Navier–Stokes system of continuity and momentum equations must be closed by initial conditions on velocity, say $\boldsymbol{u} = \boldsymbol{u_0}$ for $x \in \Omega$ and $t = 0$, and boundary conditions on the domain boundary, for all $t > 0$. Mathematically admissible boundary conditions are of either Dirichlet or Neumann type

$$\boldsymbol{u} = \boldsymbol{g} \ \text{ on } \Gamma_D, \quad \boldsymbol{T} \cdot \boldsymbol{n} = \boldsymbol{\varphi} \ \text{ on } \Gamma_N, \tag{6}$$

respectively, where $\boldsymbol{n}$ is the unit outward normal vector on $\partial\Omega$, $\Gamma_D \cup \Gamma_N = \partial\Omega$, and either Γ_D or Γ_N may be empty. The conditions to apply are normally driven by physical considerations. For instance, for a viscous fluid ($\mu > 0$), we have to impose the homogeneous Dirichlet condition $\boldsymbol{u} = \boldsymbol{0}$ at a solid fixed boundary, like the vessel wall Γ^{w} in Figure 4. When we will consider the coupled problem between fluid and vessel wall, Γ^{w} will deform, hence the homogeneous Dirichlet condition will be replaced by $\boldsymbol{u} = \boldsymbol{w}$, where $\boldsymbol{w}$ is the (unknown) wall velocity. When dealing with an artificial boundary, that is a boundary which truncates the space occupied by the fluid (for computational reasons) like the sections Γ^{in} and Γ^{out} in Figure 4, the choice of appropriate conditions is often more delicate and should in any case guarantee the well-posedness of the resulting differential problem.

We anticipate the fact (without providing the proof) that this choice of boundary conditions, with the hypothesis that at Γ^{out} the velocity satisfies everywhere the condition $\boldsymbol{u} \cdot \boldsymbol{n} > 0$, is sufficient to guarantee that the solution of the Navier–Stokes problem exists and is continuously dependent from the data (initial solution, boundary conditions, forcing terms), provided that the initial data and the forcing term be sufficiently small.

Unfortunately, the homogeneous Neumann condition is rather unphysical for the case of a human vessel. As a matter of fact, it completely neglects the presence of the remaining part of the circulatory system. The issue of devising appropriate boundary conditions on artificial boundaries of deformable arteries is still open and is the subject of active research. A possibility is provided by coupling the Navier–Stokes equations on a specific portion of the artery with reduced models, which are able to represent, although in a simplified way, the presence of the remaining part of the circulatory system. Techniques of this type has been used and analyzed in [32], [33]. An account will be given in Section 4. Normally, on arterial sections like Γ^{in} and Γ^{out} only "averaged" data are available (mean velocity and mean pressure instead of a vector condition like that in (6)), which are therefore insufficient for a "standard" treatment of the mathematical problem. One has thus to devise alternative formulations for the boundary conditions which, on one hand, reflect the physics and exploit the available data and, on the other hand, permit to formulate a mathematically well posed problem. In these notes we will not investigate this particular aspect, which is however illustrated and analyzed in [34], [97], [98].

Now we will make some considerations on the behavior of blood flow. Most often, it is laminar. Characteristic values of the Reynolds number, $\mathrm{Re} = \frac{\rho U L}{\mu}$, where U is a representative mean flow velocity and L is a linear length of the vessel at hand, are given in Table 1. In normal physiological situations, the values of the Reynolds

number reached in the cardiovascular system do not allow the formation of full scale turbulence. Some flow instabilities may occur only at the exit of the aortic valve and

Table 1. Some representative values of velocity, vessel size, average Reynolds numbers, cross-sectional area and thickness of blood vessels.

Vessel	Number	Diameter [cm]	Area [cm^2]	Wall thickness [cm]	Velocity [cm/s]	Average Reynolds number
Aorta	1	2.5	4.5	0.2	48	3400
Arteries	159	0.4	20	0.1	45	500
Arterioles	400	0.005	$5.7 \cdot 10^7$	0.002	5	0.7
Capillaries	4500	0.0008	$1.6 \cdot 10^{10}$	0.0001	0.1	0.002
Venules	4000	0.002	$1.3 \cdot 10^9$	0.0002	0.2	0.01
Veins	40	0.5	200	0.05	10	140
Vena cava	18	3	0.15	3300	38	3300

limited to the systolic phase. In this region the Reynolds number may reach the value of few thousands only for the portion of the cardiac cycle corresponding to the peak systolic velocity, however, there is not enough time for a full turbulent flow to develop.

When departing from physiological conditions, there are several factors that may induce transition from laminar to turbulent flows. For instance, the increase of flow velocity because of physical exercise, or due to the presence of a stenotic artery or a prosthetic implant such as a shunt, may induce an increase of the Reynolds number and lead to turbulence. Smaller values of blood viscosity also raise the Reynolds number; this may happen in the presence of severe anemia, when the hematocrit drops sharply (and so does the viscosity).

The rheological behavior of blood flow is complex to describe, and is still a subject of investigation. Nonetheless, a few peculiar phenomena are worth being mentioned. Red blood cells tend to aggregate by attaching each other side by side (resembling stacks of coins) forming *rouleaux*. Under shear stress, red blood cells can deform into a variety of shapes (for instance they become ellipsoids) without modifying their volume or surface area. Both aggregation and deformability affect the rheological properties of blood flow, and, particularly, blood viscosity at low shear rates and its sedimentation velocity.

In general terms, blood is a non-Newtonian fluid. At low shear rates, viscoelastic effects become relevant. In small capillaries, at small Reynolds and Womersley number, viscous effects become predominant, whereas inertial forces become negligible. The Womersley number is defined as $\alpha = R(\omega/\nu)^{1/2}$, where R is the radius, ω is the angular frequency of the oscillatory motion and ν is the kinematic viscosity. Below a critical vessel caliber (about 1 mm), blood viscosity becomes dependent on the vessel radius and decreases very sharply. This is known as Fahraeus–Lindquist effect: red

blood cells move to the central part of the capillary whereas the plasma stay in contact with the vessel wall. This layer of plasma facilitates the motion of the red cells, thus causing a decrease of the apparent viscosity. High shear rate and increased blood cell deformation are further important factors that explain viscoelastic behavior.

Some blood diseases may severely alter the rheological behavior of blood. For instance thalassemia causes red blood cells to become less deformable. In leukemia there is an increased number of poorly deformable white blood cells. In hypertension the haematocrit increases leading to a significant high blood viscosity with elevated total plasma protein, albumin, globulin and fibrinogen. See [56].

To account for these phenomena we have to abandon the Newtonian law (4). In *generalized Newtonian fluids*, the viscosity μ is assumed to depend on the shear rate $\dot{\gamma}$, a measure of the rate of shear deformation. For a simple shear flow in a straight channel (see Figure 5), $\dot{\gamma} = U/h$ is just the gradient of velocity. More in general, $\dot{\gamma} = \sqrt{2\,\mathrm{tr}(\boldsymbol{D}(\boldsymbol{u}))^2}$.

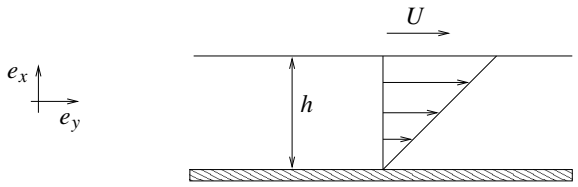

Figure 5. Schematic example of a simple shear flow in a straight channel.

A simple model is given by the so-called *Power-Law* where n is named the power-law index. The flow is *shear thinning* if $n < 1$ and *shear thickening* if $n > 1$. (Shear thinning fluids are those for which viscosity decreases as the shear rate increases.) The Prandtl–Eyring model, $\mu(\dot{\gamma}) = \mu_0 \sinh^{-1}(\lambda\dot{\gamma})/\lambda\dot{\gamma}$ where λ is a material constant, the Powell–Eyring model, $\mu(\dot{\gamma}) = \mu_\infty + (\mu_0 - \mu_\infty)\sinh^{-1}(\lambda\dot{\gamma})/\lambda\dot{\gamma}$, the Cross-model $\mu(\dot{\gamma}) = \mu_\infty + (\mu_0 - \mu_\infty)/(1 + (\lambda\dot{\gamma})^n)^{-1}$, the Carreau model $\mu(\dot{\gamma}) = \mu_\infty + (\mu_0 - \mu_\infty)/(1 + (\lambda\dot{\gamma})^2)^{(1-n)/2}$, represent other noticeable examples of generalized Newtonian models.

Blood is in general modeled as a shear thinning, nonlinear viscoelastic flow.

More complicated models are the shear thinning generalized Oldroyd-B models, where $\boldsymbol{T} = -P\boldsymbol{I} + \boldsymbol{\tau}$ and $\boldsymbol{\tau}$ satisfies the differential problem

$$\boldsymbol{\tau} + \lambda_1[\dot{\boldsymbol{\tau}} - (\nabla \boldsymbol{u})\boldsymbol{\tau} - \boldsymbol{\tau}(\nabla \boldsymbol{u}^T)] = \mu(\boldsymbol{D}(\boldsymbol{u}))\boldsymbol{D}(\boldsymbol{u}) + \lambda_2[\dot{\boldsymbol{D}}(\boldsymbol{u}) - (\nabla \boldsymbol{u})\boldsymbol{D}(\boldsymbol{u}) - \boldsymbol{D}(\boldsymbol{u})(\nabla \boldsymbol{u}^T)]$$

where λ_1, λ_2 are material constants that characterize the model. For a discussion on rheological properties of blood flow we refer, e.g., to [12], [38], [39], [94], [57]. For a more thorough mathematical analysis of Oldroyb-B models see, e.g., [102], [4], [83], [68], [40], [41], [71].

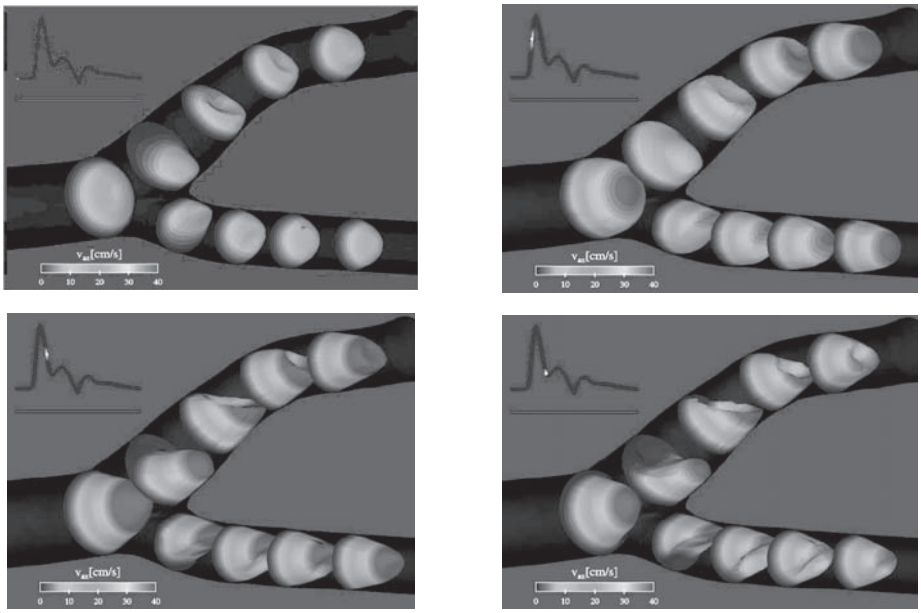

Figure 6. Velocity profiles computed in a carotid bifurcation during systole and diastole (courtesy of M. Prosi).

3. Mathematical models for local blood-flow dynamics in compliant vessels

In human physiology, the arterial walls deform under the action of the flow field. This aspect is relevant especially for large or even relatively large vessels, whereas in arterioles and capillaries the movement of the wall may be considered negligible. In the aorta, for example, the radius may vary in a range of 5% to 10% between diastole and systole. This is quite a large displacement, which affects the flow field. The fluid wall interaction problem is the responsible for the propagation of pulse pressure waves. Indeed, no propagative phenomena would otherwise occur in an incompressible fluid like blood. This interaction problem is a particular instance of the more general fluid-structure interaction (FSI) problem (the solid structure being here the vessel wall). It is indeed a rather complex one, since the time scales associated to the interaction phenomena are two orders of magnitude greater than those associated to the bulk flow field.

The vascular wall has a very complex nature; devising an accurate model for its mechanical behavior is rather difficult. Its structure is indeed formed by many layers with different mechanical characteristics [38], [48]. The most important are the endothelium (of about 2 microns, with anti-adhesive function), the tunica intima (of 10 microns, made of connective tissue), the internal elastic lamina, of 2 microns,

the media (of about 300 microns, with structural functions) and the adventitia, where the vasa vasorum stand (see Figure 7). Unfortunately, experimental results obtained by specimens are only partially significant. Indeed, the vascular wall is a living tissue with the presence of muscular cells which contribute to its mechanical behavior. It may then be expected that the dead tissue used in the laboratory will have different mechanical characteristics than the living one. Moreover, the arterial mechanics depends also on the type of the surrounding tissues, an aspect almost impossible to reproduce in a laboratory. It is the role of mathematical modeling to find reasonable

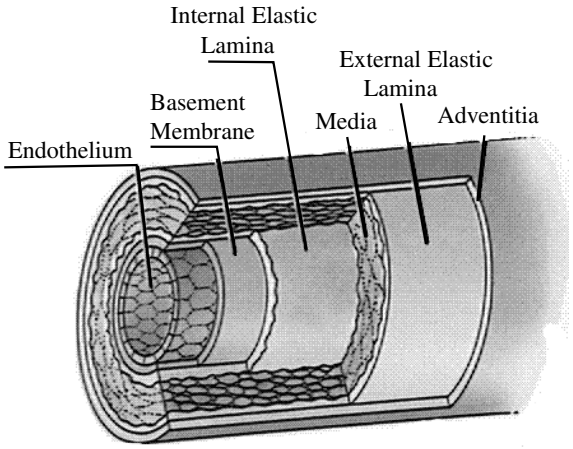

Figure 7. The vessel wall is formed by many layers made of tissues with different mechanical characteristics. Image taken from "Life: the Science of Biology" by W.K. Purves et al., fourth edition, published by Sinauer Associates Inc. and W.H. Freeman and Company.

simplifying assumptions by which major physical characteristics remain present, yet the problem becomes amenable to numerical analysis and computational solution.

The geometry of a portion of an artery where no branching is present may be described by using a curvilinear cylindrical coordinate system (r, θ, z) with the corresponding base unit vectors $\boldsymbol{e}_r$, $\boldsymbol{e}_\theta$, and $\boldsymbol{e}_z$, where $\boldsymbol{e}_z$ is aligned with the axis of the artery, as shown in Figure 10. (In this figure, R indicates the radius of the lumen.) Clearly, the vessel structure may be studied using full three dimensional models, which may also account for its multilayered nature. However, it is common practice to resort to simplified 2D or even 1D mechanical models in order to reduce the overall computational complexity when the final aim is to study the coupled fluid-structure problem. A 2D model may be obtained by either resorting to a shell-type description or considering longitudinal sections ($\theta = \text{const.}$) of the vessels. In the first case we exploit the fact that the effective wall thickness is relatively small to reduce the whole structure to a surface. A rigorous mathematical derivation (for the linear case) may be found in [15]. In the second case we neglect the variations of

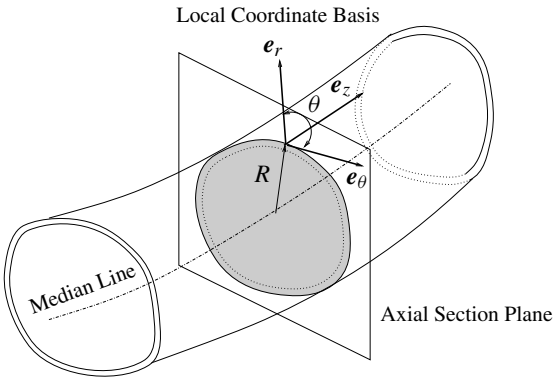

Figure 8. A model of a "realistic" section of an artery with the principal geometrical parameters.

the stresses in the circumferential direction. In this way we are able to eliminate all terms containing derivatives with respect to θ in the equations and we may consider each plane $\theta = \text{const.}$ independently. The resulting displacement field will depend only parametrically on θ. If, in addition, we assume that the problem has an axial symmetry (which implies the further assumption of a straight axis) the dependence on θ is completely neglected. In this case, also the fluid would be described by a 2D axi-symmetric model (see [25]).

The simplest models, called 1D models, are derived by making the same assumption on the wall thickness made for the shell model, yet starting from a 2D model. The structure will then be represented by a line on a generic longitudinal section. Even with all these simplifying assumptions an accurate model of the vessel wall mechanics is rather complex.

A three-dimensional model that describes the complete coupled system made of the equations of blood flow and those for the vessel wall deformation can be derived by adopting a coupled Eulerian–Lagrangian approach (differently to what done in Section 2 where the vessel walls were considered as being rigid).

With this purpose, we denote by $\hat{\Omega}$ a reference domain (corresponding, e.g., to a specific portion of an arterial vessel at rest, or else at an initial time). We write $\bar{\hat{\Omega}} = \bar{\hat{\Omega}}^s \cup \bar{\hat{\Omega}}^f$, where $\hat{\Omega}^f$ is the portion of the domain occupied by the fluid (i.e. the lumen) while $\hat{\Omega}^s$ corresponds to the portion of the solid vessel wall (see Figure 9 for a two dimensional representation). In a given time interval $[0, T]$ the domain deformation is described through a couple of functions:

$$L^s : \hat{\Omega}^s \times [0, T] \to \Omega^s(t), \quad A^f : \hat{\Omega}^f \times [0, T] \to \Omega^f(t),$$

where $\Omega^s(t)$ denotes the domain occupied by the solid (the vessel wall) and $\Omega^f(t)$ that occupied by the fluid at time t. The computational domain in which we aim at solving the coupled fluid-wall problem at time t is then $\Omega(t)$ s.t. $\bar{\Omega}(t) = \bar{\Omega}^s(t) \cup \bar{\Omega}^f(t)$. Note

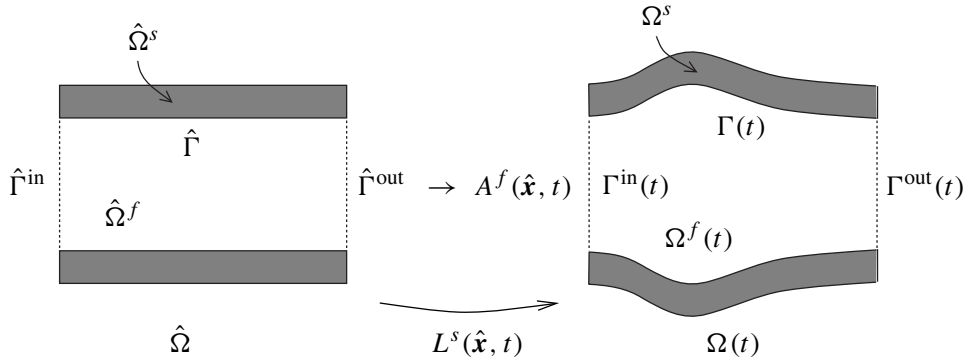

Figure 9. Parametrization of the domain.

that the boundary $\partial\Omega(t)$ of $\Omega(t)$ is made of a physical boundary (the external surface of the vessel wall, that has deformed) plus a virtual boundary (the vertical walls in the domain of Figure 9) that has not changed its position from its reference state. In fact, L^s is the Lagrangian transformation of the solid domain: the domain displacement is described by the law $\boldsymbol{\eta}(\hat{\boldsymbol{x}}, t) = L^s(\hat{\boldsymbol{x}}, t) - \hat{\boldsymbol{x}}$ for all $\hat{\boldsymbol{x}} \in \hat{\Omega}^s$, and the velocity of any point $\hat{\boldsymbol{x}}$, given by $\partial_t L^s(\hat{\boldsymbol{x}}, t) = \partial_t \boldsymbol{\eta}(\hat{\boldsymbol{x}}, t)$, is denoted by $\dot{\boldsymbol{\eta}}(\hat{\boldsymbol{x}}, t)$.

Within the fluid domain $\Omega^f(t)$, A^f is a transformation such that $A^f|_{\hat{\Gamma}} = L^s|_{\hat{\Gamma}}$ but which otherwise does not follow the material trajectories. The set of transformation $\{L^s, A^f\}$ is in fact an *Arbitrary Lagrangian Eulerian transformation* (ALE) that, at each time t, is capable to retrieve the actual position of the computational domain $\Omega(t)$ starting from the reference domain $\hat{\Omega}$. Let us denote by

$$\boldsymbol{F}^s(\hat{\boldsymbol{x}}, t) = \nabla_{\hat{\boldsymbol{x}}} L^s(\hat{\boldsymbol{x}}, t) = \boldsymbol{I} + \nabla_{\hat{\boldsymbol{x}}} \boldsymbol{\eta}(\hat{\boldsymbol{x}}, t) \quad \text{and} \quad \boldsymbol{F}^f(\hat{\boldsymbol{x}}, t) = \nabla_{\hat{\boldsymbol{x}}} A^f(\hat{\boldsymbol{x}}, t)$$

the gradients of the two maps, called the *deformation tensors*, and by

$$J^s(\hat{\boldsymbol{x}}, t) = \det \boldsymbol{F}^s(\hat{\boldsymbol{x}}, t) \quad \text{and} \quad J^f(\hat{\boldsymbol{x}}, t) = \det \boldsymbol{F}^f(\hat{\boldsymbol{x}}, t)$$

their determinants. The fluid domain velocity is denoted by $\hat{\boldsymbol{w}}(\hat{\boldsymbol{x}}, t) = \partial_t A^f(\hat{\boldsymbol{x}}, t)$. Note that, still referring to the case depicted in Figure 9, on the vertical (virtual) boundaries it is $\hat{\boldsymbol{w}} \cdot \boldsymbol{n} = \boldsymbol{0}$, whereas on $\hat{\Gamma}$ we have $\hat{\boldsymbol{w}} = \dot{\boldsymbol{\eta}}$.

The structural deformation can be modeled in many different ways, as we have anticipated at the beginning of this section. Here we will consider the following model

$$\rho^s \frac{\partial^2 \boldsymbol{\eta}}{\partial t^2} - \operatorname{div}_{\hat{\boldsymbol{x}}}(\boldsymbol{F}^s \boldsymbol{\Sigma}^s) = 0 \quad \text{in } \hat{\Omega}^s, \ t > 0$$

where $\boldsymbol{\Sigma}^s$ is the second Piola–Kirchoff stress tensor. It depends on the Green-St.Venant strain tensor $\boldsymbol{E} = \frac{1}{2}((\boldsymbol{F}^s)^T \boldsymbol{F}^s - \boldsymbol{I})$, according to a constitutive law characteristic of the solid structure at hand. Typically, $\boldsymbol{\Sigma}^s = \frac{\partial \boldsymbol{\Psi}}{\partial \boldsymbol{E}}$, where $\boldsymbol{\Psi}$ is the density

of a given elastic energy. Finally, ρ^s is the density of the structure in the reference configuration. By combining this equation with the Navier–Stokes equations (2)–(3) for the fluid we end up with the following coupled fluid-structure problem, for all $t > 0$:

$$\hat{\boldsymbol{w}} = H(\dot{\boldsymbol{\eta}}|_{\hat{\Gamma}}) \quad \text{in } \hat{\Omega}^f, \quad \boldsymbol{w} = \hat{\boldsymbol{w}} \circ (A^f)^{-1}, \tag{7}$$

$$\rho^f \frac{\partial \boldsymbol{u}}{\partial t|_{\hat{\boldsymbol{x}}}} + \rho^f (\boldsymbol{u} - \boldsymbol{w}) \cdot \nabla \boldsymbol{u} + \operatorname{div}(\boldsymbol{T}^f) = \rho^f \boldsymbol{f} \quad \text{in } \Omega^f(t), \tag{8}$$

$$\operatorname{div}(\boldsymbol{u}) = 0 \quad \text{in } \Omega^f(t), \tag{9}$$

$$\rho^s \frac{\partial^2 \boldsymbol{\eta}}{\partial t^2} - \operatorname{div}_{\hat{\boldsymbol{x}}}(\boldsymbol{F}^s \boldsymbol{\Sigma}^s) = 0 \quad \text{in } \hat{\Omega}^s, \tag{10}$$

$$\boldsymbol{u} = \dot{\boldsymbol{\eta}} \circ (L^s)^{-1} \quad \text{on } \Gamma(t), \tag{11}$$

$$\boldsymbol{F}^s \boldsymbol{\Sigma}^s \cdot \hat{\boldsymbol{n}}^s = J^f \boldsymbol{T}^f \cdot (\boldsymbol{F}^f)^{-T} \cdot \hat{\boldsymbol{n}}^s \quad \text{on } \hat{\Gamma}, \tag{12}$$

where $\hat{\boldsymbol{n}}^s$ denotes the outward unit vector on $\hat{\Gamma}$, $\frac{\partial}{\partial t|_{\hat{\boldsymbol{x}}}}$ represents the ALE time derivative (see [75]) and $H(.)$ denotes any continuous extension operator from $\hat{\Gamma}$ to the fluid domain $\hat{\Omega}^f$ (for instance the harmonic extension, or else the extension by the linear elasticity operator).

This coupled problem needs to be completed with the initial conditions on $\boldsymbol{u}$, $\boldsymbol{\eta}$ and $\dot{\boldsymbol{\eta}}$ as well as by suitable boundary conditions on $\partial\Omega^s(t)\backslash\Gamma(t)$ and $\partial\Omega^f(t)\backslash\Gamma(t)$.

At the best of our knowledge, a complete mathematical analysis of the coupled fluid-structure problem (7)–(12) is not available yet. In the steady case, for small enough applied forces, existence of regular solutions is proven in [44]. In the unsteady case, local solvability in time is proven in the simple case where the structure is a collection of rigid moving bodies in [45]. See also [27]. Formulations based on optimal control on simpler models have been investigated, e.g., in [55], [72], [66], [67], [103], [104].

As previously mentioned, simpler models than (10) can be adopted to describe the vessel deformation. Of special interest are models based on a single spatial coordinate, the one along the longitudinal axis, which usually describes the radial deformation of the vessel wall. These models are based on the following further simplifying assumptions.

Small thickness and plain stresses. The vessel wall thickness h is sufficiently small to allow a shell-type representation of the vessel geometry. In addition, we will also suppose that it is constant in the reference configuration. The vessel structure is subjected to plain stresses.

Cylindrical reference geometry and radial displacements. The reference vessel configuration is described by a circular cylindrical surface with straight axes. Indeed, this assumption may be partially dispensed with, by assuming that the reference configuration is "close" to that of a circular cylinder. The model here derived may be supposed valid also in this situation. The displacements are only in the radial direction.

Small deformation gradients. We assume that the deformation gradients are small, so that the structure basically behaves like a linear elastic solid and $\frac{\partial R}{\partial \theta}$ and $\frac{\partial R}{\partial z}$ remain uniformly bounded during the motion.

Incompressibility. The vessel wall tissue is incompressible, i.e. it maintains its volume during the motion. This is a reasonable assumption since biological tissues are indeed nearly incompressible.

Under the above assumptions we can derive the following one dimensional model that describes the radial displacement $\boldsymbol{\eta} = \eta \boldsymbol{e}_r$ of the arterial wall (see [75]):

$$\rho^s \frac{\partial^2 \eta}{\partial t^2} - a \frac{\partial^2 \eta}{\partial z^2} + b\eta - c \frac{\partial^3 \eta}{\partial t \partial z^2} = g, \quad 0 < z < L, \ t > 0, \tag{13}$$

where z denotes the longitudinal space coordinate (aligned along the vessel axis), L the length of the vessel at rest, while a, b and c are suitable coefficients which depend on material properties. Precisely:

$$a = \frac{\sigma_z}{h}, \quad b = \frac{E}{(1 - \varsigma^2) R_0^2},$$

while c is a positive coefficient that accounts for viscoelastic effects, R_0 is the radius of the cylindrical vessel at rest and h is the thickness of the vessel wall at rest, ς is the Poisson ratio, E is the Young modulus, while σ_z is the magnitude of the longitudinal stress.

The first term in (13) models the inertia, the second one the shear, the third one the elasticity, the fourth one the viscoelastic damping. Finally, g accounts for the forcing terms.

When the one-dimensional wall model (13) is used instead of (10), the coupled fluid-structure model is made of equations (7)–(9), plus the equilibrium equation (13) where the source term g is the projection along the radial direction of the normal stress of the fluid on the right hand side of (12), that is $g = J^f \boldsymbol{T}^f \cdot (\boldsymbol{F}^f)^{-T} \cdot \hat{\boldsymbol{n}}^s \cdot \boldsymbol{e}_r$; the equation (11) now reads $\boldsymbol{u} \circ A^f = \dot{\eta} \boldsymbol{e}_r$ on $\hat{\Gamma}$.

When supplemented by suitable boundary and initial conditions, this coupled system satisfies an a priori estimate stating that the kinematic energy of the fluid plus the elastic energy of the 1D vessel is controlled by the initial data and the source term (see [75]). A result of existence of strong solutions in the case of periodic conditions in space is given in [5].

The numerical solution of a coupled fluid-structure nonlinear problem like (7)–(12) (or that discussed above based on the one dimensional model (13) for the radial vessel deformation) poses many challenges. After space discretization (e.g. by the finite element method, see [77]) one obtains a coupled nonlinear algebraic system.

Since the density of the structure is comparable to that of the fluid, the stability of numerical simulations of fluid-structure interactions relies heavily on the accuracy in solving the nonlinear coupled problem at each time step [23], [59], [60], [70], [88].

Ideally, implicit schemes should be used as they would guarantee energy conservation (up to the dissipation terms) and therefore numerical stability. This is outlined on a simplified fluid-structure interaction problem in [13], where implicit and staggered algorithms are analyzed by taking into account the so-called added-mass effect. In particular it is shown that numerical instabilities may occur when using loosely coupled time-advancing schemes. To account for the nonlinear coupling between fluid and structure, common strategies rely on fixed point methods [14]. Several ad-hoc variants have been proposed, including steepest descent algorithms in [88], Aitken-like acceleration formulas [63], [64], and transpiration boundary conditions [23] to avoid the computation of the fluid matrices at each sub-iteration. Yet, in general, these methods are slow, and in some cases may even fail to converge [70], [13], [25]. A more radical approach consists of using Newton based methods, owing to their potentially faster convergence [25], [29], [46], [61]. However, since they demand the evaluation of the Jacobian associated to the fluid-solid coupled state equations, a critical step is the evaluation of the *cross* Jacobian [93], which expresses the sensitivity of the fluid state to solid motions. This evaluation can be made inexactly, either by resorting to finite difference approximation of derivatives (see, e.g., [93]), or by barely replacing the tangent operator of the coupled system with a simpler one [42], [43]. However, either approximation may seriously compromise the convergence rate. Acceleration techniques using Krylov spaces have been proposed in [26], [46], [62]. A Newton method with exact Jacobian has been investigated both mathematically and numerically in [29].

Methods based on a fractional-step solution of the coupled system are proposed in [30]. In this case, the coupling conditions (11) and (12) are not exactly enforced. The diffusion term of the momentum equations are advanced first from the time step t^n to $t^{n+1} = t^n + \delta t$ ($\delta t > 0$ being the time-step), and the normal component of the continuity equation (11) is imposed; then the equation for the solid structure (10) is coupled with the projection step of the Navier–Stokes equations, and the stress continuity equation (12) is enforced.

Another strategy is mutuated from domain decomposition techniques (see [78]) and is proposed in [24]. The global coupled problem (7)–(12) is reduced to a (generally nonlinear) interface equation, the so-called pseudo-differential *Steklov–Poincaré* equation, where the only unknown is the displacement of the interface separating the fluid and the structure. At any time-step, after space discretization, the aim is to exploit the physically decoupled structure of the original problem, in such a way that the solution is obtained through a sequence of independent solves involving each subproblem separately.

A preliminary approach in this direction can be found in [88], [65], where the coupling between Stokes equations and a linearized shell model is considered. The analysis of the Steklov–Poincaré operators associated to the fluid and shell models is developed, and a Richardson scheme in which the shell operator acts as preconditioner is proposed and tested. Another instance is presented by Mok and Wall [63], who proposed an iterative substructuring method requiring, at each step, the independent

solution of a fluid and a structure subproblem, supplemented with suitable Dirichlet or Neumann boundary conditions on the interface.

As it was observed, one of the advantages of the Steklov–Poincaré approach is that the whole problem is reduced to an equation involving only interface variables. In this respect, it can be regarded as a special instance of *heterogeneous domain decomposition*, arising whenever in the approximation of certain physical phenomena two (or more) different kinds of boundary value problems hold within two disjoint subregions of the computational domain (see, e.g., [78]). The key to efficiency is to set up convenient preconditioners for the discretized Steklov–Poincaré equation, as done in [24]. In Figure 10 we plot the numerical simulation of the wall deformation of a straight cylindrical vessel at two different time-instants of the cardiac beat. The gray scales indicate pressure iso-values. In Figure 11 the same kind of simulation is reported for a carotid artery. Arrows indicate the blood velocity field.

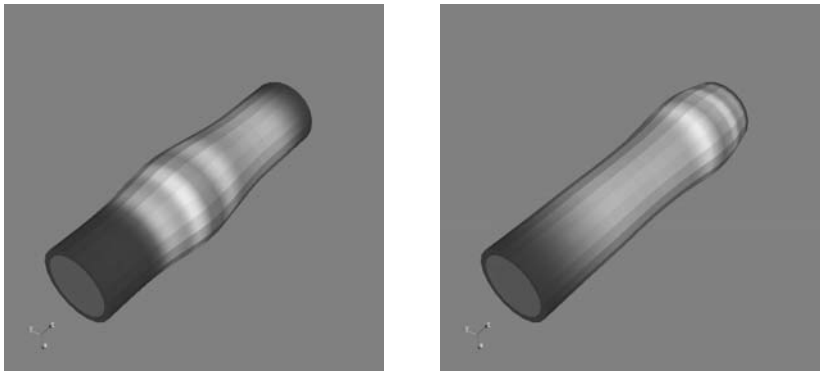

Figure 10. Pressure wave propagation in a straight vessel (simulation by G. Fourestey).

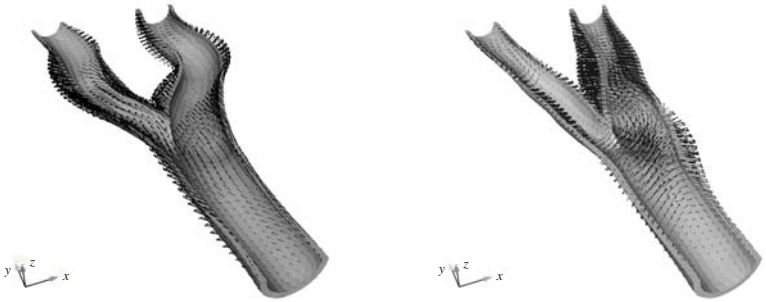

Figure 11. (From [24]). Structure deformation of a carotid artery and velocity at time $t = 10\,\text{ms}$ (left) and $t = 20\,\text{ms}$ (right).

4. Modeling the whole circulatory system

So far we have shown how to set-up mathematical models to simulate local phenomena. In fact, a change of perspective is necessary if we want to investigate processes that occur on the vascular tree at large: instances include the propagation of the pressure pulse from heart to periphery, the self-regulation process that governs the dynamics of blood solutes (oxygen, drugs, etc.), the aging effects on the arterial elasticity, the overload on the heart induced by the implant of an endovascular prosthesis, the regulating processes that the body activates to contrast severe changes in external conditions, etc.

Modeling these processes requires to integrate multiple scales in space and time, and to account for the correlation between actions and reactions in different cardiovascular compartments.

The simulation of a large part of the circulatory system by solving the three-dimensional Navier–Stokes equations everywhere would require the availability of a large set of morphological data (quite difficult to obtain), not to mention the computational costs that would be out of reach. On the other hand, the richness of detail intrinsic to a 3D model may not be necessary when one is primarily interested in the simulation of global flow features. Rather, suitable hierarchies of reduced models, made of networks of 1D pipes and lumped parameter circuits carrying different level of detail, can be developed to provide sufficiently reliable answers to our questions.

By exploiting the fact that, at least locally, an artery is a quasi-cylindrical vessel and that blood flows mainly in the axial direction, we build a simplified model that neglects the transversal components of the velocity, assumes that the wall deforms along the radial direction only, and describes the fluid-structure interaction blood flow problem in terms of two scalar functions: the measure $A(z,t)$ of a generic axial section $\mathcal{A}(z)$ of the vessel and the mean flux $Q(z,t) = \int_{\mathcal{A}(z)} u_z d\sigma$. Here, z indicates the axial coordinate (see Figure 12, left). Under simplifying, yet realistic, hypotheses the following one dimensional (1D) model is obtained [75]:

$$\begin{aligned} &\frac{\partial A}{\partial t} + \frac{\partial Q}{\partial z} = 0, \\ &\frac{\partial Q}{\partial t} + \frac{\partial A}{\partial \rho}\frac{\partial p}{\partial A} - \alpha \bar{u}_z^2 \frac{\partial A}{\partial z} + 2\alpha \bar{u}_z \frac{\partial Q}{\partial z} + K_R\Big(\frac{Q}{A}\Big)Q = 0, \end{aligned} \qquad z \in (0, L),\ t > 0 \quad (14)$$

which describes the flow of a Newtonian fluid in a compliant straight cylindrical pipe of length L. Here, $\bar{u}_z = A^{-1}\int_{\mathcal{A}} u_z d\sigma$ is the mean axial velocity and $\alpha = (A\bar{u}^2)^{-1}\int_{\mathcal{A}} u_z^2 d\sigma$ is the *Coriolis* coefficient. The pressure is assumed to be function of A according to a constitutive law that specifies the mechanical behavior of the vascular tissue. Different models can be obtained by choosing different pressure-area laws. Finally, K_R is a parameter accounting for the viscosity of the fluid. For the analysis of the hyperbolic system (14) see [75] and [10].

In this simple (and most popular) one dimensional model the vessel mechanics is overly simplified. In practice, it is reduced to an algebraic relationship between the

mean axial pressure (more precisely the average intra-mural pressure) and the area of the lumen. However, one may also account for other mechanical properties such as viscoelasticity, longitudinal pre-stress, wall inertia. In the latter case, the relation between pressure and vessel area is governed by a differential equation. Yet, it is still possible, at a price of some simplifications, to recover again a system of two partial differential equations [35], [33]. By so doing, the wall inertia introduces an additional dispersive term, while viscoelasticity contributes with a dissipation term. The treatment of these additional terms is problematic as further boundary conditions would be required. However, for physiological situations inertia and viscoelastic effects are not very important. Further improvements account for tapering and curvature (the latter cannot be neglected in arterial vessels such as the coronaries, the aortic arch, etc.). The model becomes fairly more involved, an account is given, e.g., in [54], [84]. At some extent, the arterial system in its entirety can be regarded as a network

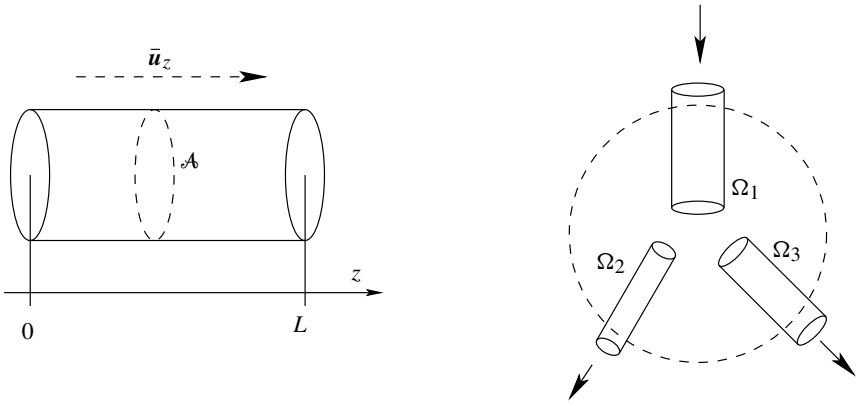

Figure 12. Left: Representation of an arterial cylindrical segment. Right: Sketch of a bifurcation

of 1D pipes, each of these being modeled by the hyperbolic system (14) (or its variants that account for curved vessels), supplemented by suitable matching conditions at the branching or bifurcation points (like in Figure 12, right) ensuring mass and energy conservation (see [75]). Its mathematical investigation would require the analysis of nonlinear hyperbolic systems on networks (see, e.g., [19], [53]).

The resulting network of one dimensional hyperbolic models are very well suited to describe the propagation of waves (the *pulse*), a phenomenon generated by the interaction between blood flow and compliant vessel wall and intrinsically related to the elastic properties of the arteries. In Figure 13 we report some snapshots of the numerical solution obtained by simulating with 1D models the application of a prosthesis at the abdominal bifurcation to cure an aneurysm. Figures on the top represents the case of an endo-prosthesis made with material softer that the vascular tissue. On the bottom the case where the prosthesis is stiffer. The presence of a strong back-reflection in the latter case is evident. When the reflected wave reaches the

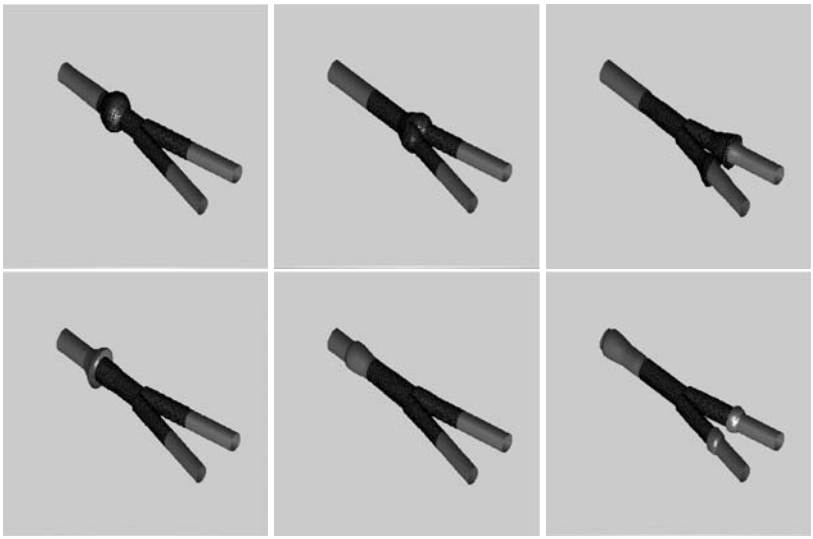

Figure 13. (from [36]). Snapshots of the simulation of a vascular bifurcation with a prosthesis, carried out with a 1D model. The three pictures in the top row illustrate the case of a prosthesis softer than the arterial wall. The most relevant reflection is at the distal interface between the prosthesis and the vessels (right). At he bottom row the results obtained using the same boundary data but with a prosthesis stiffer than the vascular wall. The most relevant reflection is at the proximal interface between the vessel and the prosthesis (left) and it back propagates up to the heart.

heart it may induce a pressure overload. These results may guide the design of better prostheses. A more complete 1D network, like the one including the largest 55 arteries shown in Figure 14, left, may be adopted for a more sound numerical investigation of the systemic dynamics.

Peripheral circulation in smaller arteries and capillaries may be accounted as well by *lumped parameter models*.

Here, a further simplification in the mathematical description of the circulation relies on the subdivision of the vascular system into *compartments*, according to criteria suited for the problem at hand. The blood flow as well as the other quantities of interest are described in each compartment by a set of parameters, typically the average flux and pressure in the compartment, depending only on time. The mathematical model is then made of a system of algebraic and ordinary differential equations in time that govern the dynamics of each compartment and their mutual coupling. Often, these models are called (with a little abuse of notation) 0D *models* ("zero" because there is no space variability any longer). In this way, large parts of the circulation system (if not all) can be modeled. The level of detail can be varied according to the problem needs.

A useful way of representing lumped parameter models of the circulation is based

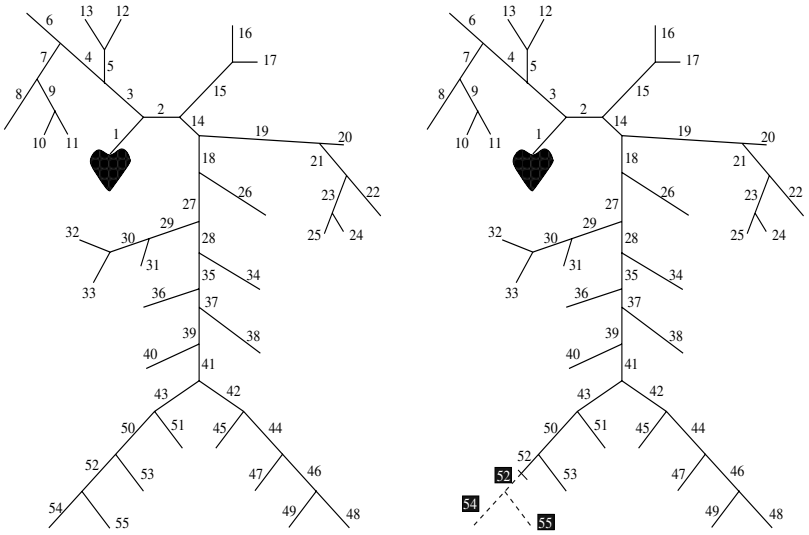

Figure 14. Arterial tree composed of a set of 55 straight vessels, described by 1D models (see [100]). On the right a pathological case, in which some of the vessels are supposed to be completely occluded.

on the analogy with electric networks, where the flow rate is represented by the electric current and pressure by the voltage. The equations coupling the different compartments are given by the *Kirchhoff balance laws*, which derive from the continuity of mass and pressure. The effects on blood dynamics due to the vascular compliance is here represented by means of capacitances. Similarly, inductances and resistances represent the inertial terms and the effect of blood viscosity, respectively (see e.g. [37] and references therein). Figure 15 illustrates different electrical schemes that may be used to describe blood flow in a passive compartment. Exploiting the same analogy, it is also possible to devise a lumped parameter representation of the heart. Since, as stated in [69], Chapter 13, left ventricle and arterial circulation represent two mechanical units that are joined together to form a coupled biological system, we need to couple the 1D model with a model of the heart (or at least of the left ventricle), for instance a lumped parameter model. The opening of the aortic valve is driven by the difference between the ventricular and the aortic pressure, P_v and P_a, while the closing is governed by the flux. The electric analog of each ventricle is given in Figure 16 where the presence of heart valves has been taken into account by *diodes* which allow the current flow in one direction only. A simple ordinary differential equation that accounts for this dynamics reads $\frac{d}{dt}(C(t)P_v(t)) = -M_Q(t)$, where Q represents the incoming flow rate, and M_Q is the action exerted by the contraction of the cardiac muscle. Precisely, $M_Q = \frac{dV_0}{dt}$, V_0 being the reference volume that changes in time because of the variation of the length of the muscle fibers. The action

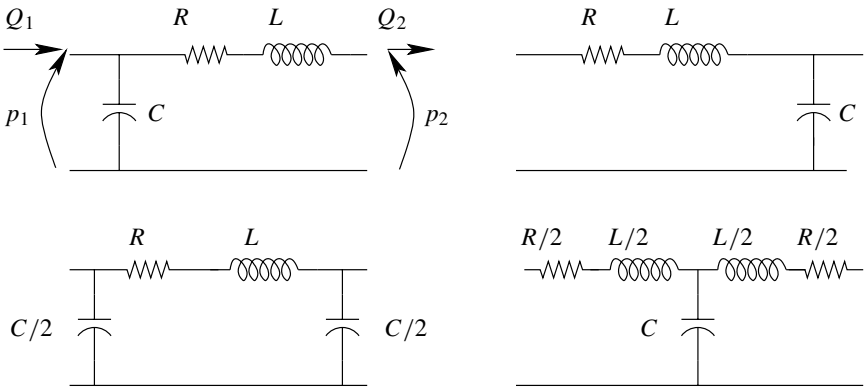

Figure 15. (From [36]). Four possible lumped parameters representation of a compliant vessel in terms of electrical circuits. The four cases differ for the state variables and the upstream/downstream data to be prescribed. The letters R, L, C indicate resistances, inductances and capacitances, respectively, while Q and p denote flow rate and pressure.

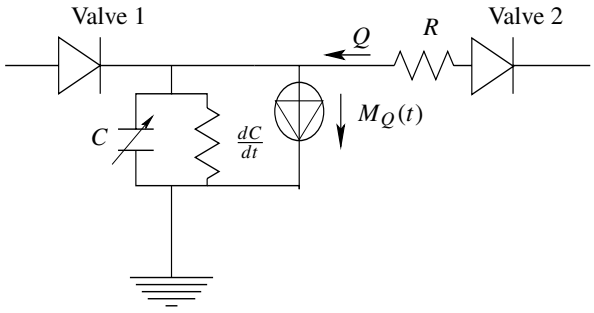

Figure 16. (From [36]). Network for the lumped parameter model of a ventricle.

of the aortic valve is described by setting $Q = 0$ when $P_a > P_v$, $P_a = P_v - RQ$ if $Q > 0$. For more details about this model, see [37]. More sophisticated ODE models are available, such as the visco-elasto-plastic model in [7].

From a mathematical standpoint, a general representation of lumped parameters models is a Differential-Algebraic-Equations (DAE) system in the form

$$\begin{aligned} &\frac{d\mathbf{y}}{dt} = B(\mathbf{y}, \mathbf{z}, t) \quad t \in (0, T] \\ &G(\mathbf{y}, \mathbf{z}) = 0 \end{aligned} \tag{15}$$

supplemented with the *initial condition* $\mathbf{y}|_{t=t_0} = \mathbf{y}_0$. Here, $\mathbf{y}$ is the vector of *state variables* while $\mathbf{z}$ are the other variables of the network which do not appear as time derivative, G is a set of algebraic equations that derive from Kirchhoff laws. If $\frac{\partial G}{\partial \mathbf{z}}$ is nonsingular, then by the implicit function theorem the DAE system (15) can be

formulated in terms of $\boldsymbol{y}$ solely. By coupling together schemes like those illustrated in Figure 15 for the different compartments and schemes like that in Figure 16 (or more sophisticated ones) to model the blood supply from heart it is possible to derive a lumped parameter model of the whole circulatory system. An example is provided by the four-compartment model illustrated in Figure 17, which comprises a lumped description of heart, lungs, arterial and venous circulation. Unfortunately, the param-

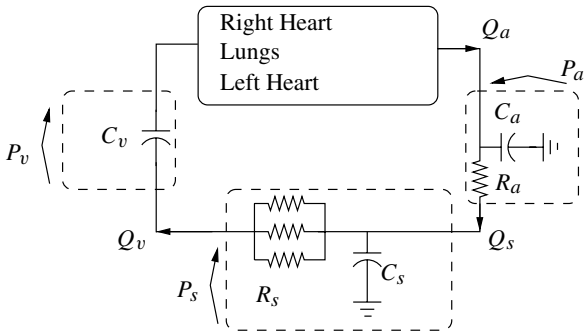

Figure 17. (From [36]). A four compartment description of the vascular system with self-regulating controls.

eters that govern the model, like resistances and compliances, can hardly be obtained from measurements or other means. In fact the circulatory system ensures a correct blood supply to organs and tissues in very diverse situations, at rest as well as after a long run. This is possible thanks to self regulating mechanisms. One of such mechanisms ensures that the arterial pressure is maintained within a physiological range (about 90–100 mmHg). Indeed, if pressure falls below this range, the oxygenation of the peripheral tissues would be seriously affected; on the other hand, a high arterial pressure would induce vascular diseases and heart overload. This regulation mechanism is called *baroreflex effect* and is described, for instance, in [49] and [52]. The elements of the feedback baroreceptor loop are a set of *baroreceptors* located in the carotid arteries and the aortic arch, which transmit impulses to the brain at a rate increasing with the arterial pressure, the *parasimpathetic nervous system*, which is excited by the activity of baroreceptors and can slow down the heart rate, and the *simpathetic nervous system*, which is inhibited by the baroreceptors and can increase the heart rate. It controls also the venous pressure and the systemic resistance.

Another ingredient of the self-regulating capabilities of the arterial system is the so called *chemoreflex effect*, a mechanism able to induce capillaries dilation and opening when an increment of oxygen supply is required by the organs, for instance during heavy exercise.

Chemoreflex and baroreflex effects can be included in the differential models presented so far through another coupled ODE system that models these feedback mechanisms (see, e.g., [21], [20] and the references therein).

Being able to adopt equations in different geometrical dimensions (3D, 1D and 0D, as we have illustrated thus far) provides tremendous new opportunities for modeling the circulatory system, but, at the same time, poses severe mathematical challenges. Multiscale geometrical systems can be set-up using 3D models of the type (7)–(12) to provide a complete description of the flow-field and 3D vessel deformation in specific districts (such as, e.g., the carotid bifurcation, the aortic arch, a stenosed coronary artery) combined with a network of 1D models like (14), one for every compliant vessel apt at providing average values of flow-rate and pressure on each vessel axial section. The rest of the system – the heart, the venous system, the capillary bed, the small circulation – may be accounted for by either prescribing appropriate "boundary" conditions at the terminal vessels or, more realistically, by adopting 0D lumped parameter (ODE) models capable of describing the feedback effects due to peripheral circulation. With this approach, difficulties arising from the treatment of boundary conditions for 3D model (mentioned in Section 2) are naturally handled.

From a mathematical standpoint, the use of such a geometrical multiscale model calls for the set up of matching conditions between the various submodels. These conditions should ensure the conservation of mass and stresses at the interfaces between heterogeneous submodels. This is not obvious to achieve, since the submodels live in spaces of different dimensions, are made of equations of different type and number, and feature different kind of unknown variables. Furthermore, the multiple geometrical models coupled with the continuity conditions at interfaces should hopefully define a globally well-posed mathematical problem.

The analysis of the complete system is very difficult, though. Partial results are available on the coupling of 3D and 0D models, and of 1D and 0D, see [33], [32], [81]. An account is given in [37].

So far, we have described the heart ventricle functionality by a simple 0D model. Clearly, this is an overly simplified approach. In fact, the development of a mathematical model for describing the electrical, mechanical and biochemical function of the heart and its coupling with the ventricular blood dynamics is tremendously challenging.

The changes in the electrical potential across the muscle cell outer membrane triggers the myocardium, whose contraction prompts ejection of blood from the ventricles. Electric current flows into a cell, raises the potential and initiates the wave propagation along the cells, which are connected by gap junction proteins. The entire myocardium is activated within 50 ms and the mechanical contraction lasts for about 300 ms.

From a numerical perspective, the difficulty is represented by the need of coupling efficiently large deformation mechanics, electrical excitation and wave propagation, turbulent flow fields, which feature different characteristic spatial and temporal scales. Moreover, the electric activity of the heart influences the activation function of 1D network models like the one in Figure 13 that could be used for the systemic circulation. Reciprocally, the pressure pulse that is modeled by 1D network interacts with the cardiac electrodynamics.

Tremendous progress has been made though in the past two decades. The *immersed boundary method* was introduced by Charles Peskin in his Ph.D thesis in 1972 in order to study the fluid dynamics of heart valves, and it was then extended to become a three-dimensional model of the whole heart (see [73] and the references therein). According to Peskin, "the philosophy of the immersed boundary method is to blur the distinction between fluid dynamics and elasticity". This is accomplished by inserting in the right hand side of the momentum equation (5) a forcing term $F(\boldsymbol{x}, t) = \int_{\hat{\Omega}^s} \boldsymbol{f}(\hat{\boldsymbol{x}}, t)\delta(\boldsymbol{x} - \boldsymbol{X}(\hat{\boldsymbol{x}}, t))d\hat{\boldsymbol{x}}$ representing the forces acting on the blood flow because of the presence of a solid structure (a valve, or the cardiac fibers). The vector $\boldsymbol{f}$ denotes the density distribution of forces (whose expression depends on the mathematical model adopted to describe the structural deformation), δ is a Dyrac function, $\boldsymbol{X}$ describes the motion of the solid structure (like L^s in Section 3), and is related to the fluid velocity $\boldsymbol{u}$ by the Lagrangian relation $\partial_t \boldsymbol{X}(\hat{\boldsymbol{x}}, t)) = \boldsymbol{u}(\boldsymbol{X}(\hat{\boldsymbol{x}}, t), t), \hat{\boldsymbol{x}} \in \hat{\Omega}^s, t > 0$. Both the Eulerian and the Lagrangian variables are employed.

The development of a global cardiac model using finite elements for finite deformation mechanics equations is proposed in [87]. An anatomically based description using finite element shape functions is given, then governing equations are proposed to relate material properties to tissue behavior.

Cardiac tissue is made of discrete cells but it can be modeled as a continuum. For instance, the *bidomain model* (see, e.g., [17], [16]) consists of two interpenetrating domains that represent cells (intracellular domain) and the space surrounding the cells (extracellular domain). These two domains are assumed to co-exist at all points in the computational domain. The tissue microstructure is accounted for in the activation model through the extra-and-intra-cellular conductivity tensors. From the mathematical viewpoint, this macroscopic representation of the cardiac tissue by a reaction-diffusion system of partial differential equations can be rigorously derived by a homogeneization procedure [2], [6].

The development of realistic models for heart functioning is however far from being achieved, due to the tremendous complexity of this physical system and the induced computational complexity of the associated numerical models.

5. Mathematical models for biochemical processes

Besides the biochemical and electrical processes described so far, mathematical models can be set up to describe the transport, diffusion and absorption of biomedical components (such as oxygen, nutrients, drugs, low density lipoproteins (LDL), etc.) in the blood stream and through the different layers of the arterial wall. Numerical simulation of biochemical processes can in fact explain biochemical modifications produced by alterations in blood flow field like those occurring at outer wall of bifurcations, inner wall of curved vessels, in anastomotic junctions (as in a coronary by-pass) and stenotic arteries.

The dynamics of solutes in arteries, like dissolved gases (such as O_2) or macromolecules (such as albumin or LDL) is indeed strongly affected by the blood flow dynamics. The local transfer of mass between blood and arterial walls is functional to the transport of nutrients to cells and the removal of metabolic wastes, yet it also affects the accumulation of potentially atherogenic molecules. For instance the accumulation in the intima of LDL occurs at zones of low and oscillating wall shear stress, which seem to be correlated with the tendency to intima thickening.

The basic step for the modeling of mass transfer is the set up of a mathematical model which describes the filtration of plasma and the transfer of chemicals from the lumen to the arterial wall. The blood flow into the arterial lumen is governed by the Navier–Stokes equations (2), (5), while the filtration across the tissue layers constituting the wall can be described by a Darcy type model,

$$\bar{\boldsymbol{u}} = -\frac{K_D}{\mu}\nabla P \quad \text{with } \operatorname{div}(\bar{\boldsymbol{u}}) = 0, \tag{16}$$

where $\bar{\boldsymbol{u}}$ is the volume-averaged velocity, P is the pressure, K_D is the (Darcy) wall permeability, μ is the dynamic viscosity. On the other side, the dynamics of chemicals is generally governed by a system of advection-diffusion equations. Precisely, applying the mass conservation principle on a generic control volume, we obtain the following equation

$$\partial_t \bar{c} + \operatorname{div}\left(-D\nabla\bar{c} + \gamma\bar{\boldsymbol{u}}\bar{c}/\varepsilon\right) = 0, \tag{17}$$

where $\bar{c}$ is the volume-averaged concentration, D is the diffusivity of the chemical species at hand, $0 \le \varepsilon \le 1$ is the porosity of the considered medium; the case $\varepsilon = 1$ represents the pure fluid phase. Collisions of large molecules with the structure of the porous tissue layer result in a reduced convective transport, a phenomenon that is accounted for by using the *hindrance coefficient* $0 < \gamma \le 1$.

In the simplest *wall-free model*, the fluid dynamics and the mass transport in the arterial lumen are described by the Navier–Stokes equations (2), (5) and the advection-diffusion equation (17). At the interface between the lumen and the arterial wall (the endothelium) appropriate conditions for the volume flux (J_v) and the mass flux (J_s) are assumed:

$$\boldsymbol{u}_l \cdot \boldsymbol{n}_l = J_v \ \text{ on } \Gamma, \quad (-D_l\nabla c_l + \boldsymbol{u}_l c_l)\cdot \boldsymbol{n}_l = J_s \ \text{ on } \Gamma.$$

In this case the values of J_v and J_s are provided by experimental data ([8], [99], [95], [91]). More realistic models are the *fluid-wall* model and the *multilayer* model, both requiring suitable matching conditions describing the flux of fluid (J_v) and the flux of chemicals (J_s) between two solutions (denoted by $i = 1, 2$) separated by a semi-permeable membrane across which concentrations and fluid pressure are different, see [51], [50]. In the case of just one solute, denoting with $\delta p = p_1 - p_2$ and $\delta c = c_1 - c_2$ the driving forces across the membrane, the interface equations originally proposed

by Kedem–Katchalsky read as follows,

$$J_v(P_1, P_2, c_1, c_2) = L_P(\delta P - \delta\pi) \quad \text{with } \delta\pi = \sigma RT\delta c, \tag{18}$$

$$J_s(c_1, c_2, P_1, P_2) = \Pi\delta c + sf(c_1, c_2)J_v, \tag{19}$$

where T is the absolute temperature, while s (the sieving coefficient), L_P (the hydraulic conductivity) and Π (the permeability), R (the gas constant) are phenomenological coefficients.

In their original theory Kedem and Katchalsky provide J_v and J_s in the case of two compartments filled with a free fluid. When taking into account two heterogeneous porous media (like two continuous wall layers) permeated by solutions of different concentrations and pressures, the driving forces are still δP and δc (where c in the case of porous media represents the concentration in the fluid phase), however the phenomenological coefficients now depend on the porosity of each medium and we will call them *effective coefficients*, denoted with $L_{P,\text{eff}}(\varepsilon_1, \varepsilon_2)$, $\Pi_{\text{eff}}(\varepsilon_1, \varepsilon_2)$, $s_{\text{eff}}(\varepsilon_1, \varepsilon_2)$ respectively. This theoretical characterization is a very challenging task, see e.g. [18], [89], [90], [22]. An approach that allows a *direct* estimation of the effective coefficients is proposed in [74].

To define the mathematical problems describing the mass transfer from the lumen to the arterial wall, we label with $i = 1$ the physical quantities associated with the free fluid and with $i = 2$ the ones corresponding to the porous medium, and denote by Γ the interface between these media. Then, the fluid dynamics is governed by eqs. (2), (5) in Ω_1, eq. (16) in Ω_2, and the following conditions at the interface:

$$\boldsymbol{u}_1 \cdot \boldsymbol{n}_1 = \bar{\boldsymbol{u}}_2 \cdot \boldsymbol{n}_1 \text{ and } \bar{\boldsymbol{u}}_2 \cdot \boldsymbol{n}_1 = J_v \quad \text{on } \Gamma. \tag{20}$$

Finally, we observe that in the free fluid (corresponding to a porosity $\varepsilon_1 = 1$) the velocity of the fluid phase is equivalent to the volume averaged one. Thanks to this identification the volume averaged velocity can be referred to as $\bar{\boldsymbol{u}}_i$ in both domains. The concentration $\bar{c}_i$ of a given chemical is governed by the following problem,

$$\begin{aligned}
&\partial_t \bar{c}_i + \operatorname{div}(-D_i\nabla\bar{c}_i + \gamma_i\bar{\boldsymbol{u}}_i\bar{c}_i/\varepsilon_i) + r_i\bar{c}_i = 0, && \text{in } \Omega_i,\ i = 1, 2,\\
&(-D_1\nabla\bar{c}_1 + \gamma_1\bar{\boldsymbol{u}}_1\bar{c}_1/\varepsilon_1)\cdot\boldsymbol{n}_1 \\
&\qquad = \Pi_{\text{eff}}(\bar{c}_1/\varepsilon_1 - \bar{c}_2/\varepsilon_2) + f(\bar{c}_1/\varepsilon_1, \bar{c}_2/\varepsilon_2)J_v && \text{on } \Gamma,\\
&(-D_2\nabla\bar{c}_2 + \gamma_2\boldsymbol{u}_2\bar{c}_2/\varepsilon_2)\cdot\boldsymbol{n}_2 \\
&\qquad = -[\Pi_{\text{eff}}(\bar{c}_1/\varepsilon_1 - \bar{c}_2/\varepsilon_2) + f(\bar{c}_1/\varepsilon_1, \bar{c}_2/\varepsilon_2)J_v] && \text{on } \Gamma,
\end{aligned} \tag{21}$$

where the Kedem–Katchalsky equation (19) has been rewritten in terms of the volume averaged concentration. Finally, we observe that the multilayer model is described by a set of equations similar to (20) and (21). Precisely, its fluid dynamics part is obtained by adding to problem (20) a further domain, describing the intima, that will be coupled to the lumen and the media prescribing that the normal velocity across

the interface between these domains is continuous and equal to the flux J_v, defined in (18). Analogously, the extension of equation (21) to the multilayer case features a third advection-diffusion equation defined in the intima and coupled to the rest of the system by imposing that the total flux of chemical (namely $(-D\nabla\bar{c} + \gamma\bar{\boldsymbol{u}}\bar{c}/\varepsilon)\cdot\boldsymbol{n}$) is continuous across the interfaces and equal to J_s, defined in (19).

Besides their interest for bio-medical applications, (20) and (21) represent a difficult system of nonlinear partial differential equations whose analysis has been specifically addressed in [105], [79], [80]. Irregularities in the flow field across the arterial wall influence the concentration distribution within the wall. Figure 18 displays the concentration contours in the wall of the two different wall models at selected locations in the expanding region of the stenosis. We observe that the perturbations in the velocity field in the intima and the media affect the concentrations as well. For example in the media, the concentration in the region of high filtration velocities is slightly higher than the average value, while it is lower than the average in correspondence of low filtration velocities. More analysis and numerical simulations can be found in [105], [74]. Systems like those introduced in this section can also be applied to

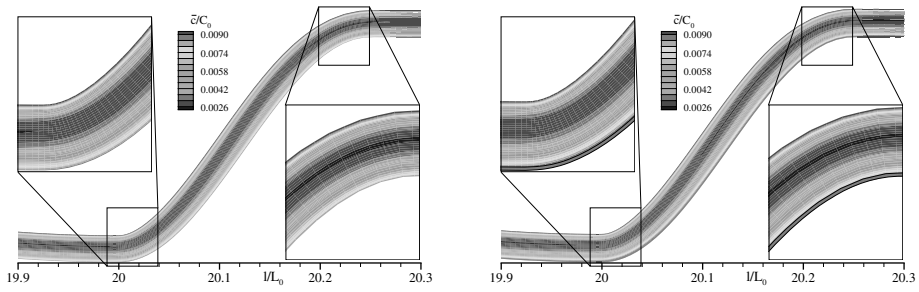

Figure 18. (From [74]). Concentration contours provided by the fluid-wall model (left) and the multilayer model (right). In the latter case, the presence of the intima is put into evidence.

the modeling of biochemical processes arising from the control of peritoneal dialysis [107], drug eluting materials [106], and artificial blood oxygenators [58].

References

[1] Agoshkov, V., Quarteroni, A., Rozza, G., Shape design in aorto-coronaric bypass anastomoses using perturbation theory. *SIAM J. Numer. Anal.* **44** (2006), 367–384.

[2] Ambrosio, L., Colli Franzone, P., Savaré, G., On the asymptotic behaviour of anisotropic energies arising in the cardiac bidomain model. *Interfaces Free Bound.* **2** (2000), 213–266.

[3] Aris, R., *Vectors, Tensors, and the Basic Equations of Fluid Mechanics*. Prentice Hall, Englewood Cliffs, NJ, 1992.

[4] Arada, N., Sequeira, A., Strong steady solutions for a generalized Oldroyd-B model with shear-dependent viscosity in a bounded domain. *Math. Mod. Meth. Appl. Sci.* **13** (9) (2003), 1303–1323.

[5] Beirão da Veiga, H., On the existence of strong solutions to a coupled fluid-structure evolution problem. *J. Math. Fluid Mechanics* **6** (2004), 21–52.

[6] Bellettini, G., Colli Franzone, P., Paolini, M., Convergence of front propagation for anisotropic bistable reaction-diffusion equations. *Asymp. Anal.* **15** (1997), 325–358.

[7] Bestel, J., Clément, F., Sorine, M., A Biomechanical Model of Muscle Contraction. *MICCAI* (2001), 1159–1161.

[8] Bratzler, R. L., Chisolm, G. M., Colton, C. K., Smith, K. A., Lees, R. S., The distribution of labeled low-density lipoproteins across the rabbit thoracic aorta in vivo. *Atherosclerosis* **28** (1977), 289–307.

[9] Campeau, L., Enjalbert, M., Lesperance, J., Vaislic, C., Grondin, C. M., Bourassa, M. G., Atheroslerosis an dlate closure of aortocpronary saphenous vein grafts; sequential angiographic studies at 2 weeks, 1 year, 5-7 year and 10-12 years after surgery. *Circulation* **68** (1983), 1–7.

[10] Canic, S., Kim, E. H., Mathematical analysis of the quasilinear effects in a hyperbolic model of blood flow through compliant axi-symmetric vessels. *Math. Models Methods Appl. Sci.* **26** (14) (2003), 1161–1186.

[11] Caro, C. G., Fitz-Gerald, J. M., Schroter, R. C., Atheroma and arterial wall shear stress. Observations, correlation and proposal of a shear dependent mass transfer mechanism for atherogenesis. *Proc. Roy. Soc. B* **177** (1971), 109–159.

[12] Caro, C. G., Pedley, T. J., Schroter, R. C., Seed, W. A., *The Mechanics of Circulation*. Oxford University Press, 1978.

[13] Causin, P., Gerbeau, J.-F., Nobile, F., Added-mass effect in the design of partitioned algorithms for fluid-structure problems. *Comput. Methods Appl. Mech. Engrg.* **194** (42–44) (2005), 4506–4527.

[14] Cervera, M., Codina, R., Galindo, M., On the computational efficiency and implementation of block-iterative algorithms for nonlinear coupled problems. *Engrg. Comput.* **13** (6) (1996), 4–30.

[15] Ciarlet, P.G., *Introduction to Linear Shell Theory*. Gauthiers-Villars, Paris 1998.

[16] Colli Franzone, P., Pavarino, L., A parallel solver for reaction diffusion systems in computational electro-cardiology. *Math. Models Methods Appl. Sci.* **14** (6) (2004), 883–912.

[17] Colli Franzone, P., Pavarino, L., Taccardi, B., Simulating patterns of excitation, repolarization and action potential duration with cardiac Bidomain and Monodomain models. *Math. Biosci.* **197** (2005), 35–66.

[18] Curry, F. R. E., Mechanics and thermodynamics of transcapillary exchange. In *Handbook of Physiology*, ed. by E. M. Renkin, American Physiological Society, 1984.

[19] Dáger, R., Zuazua, E., Controllability of tree-shaped networks of vibrating strings. *C. R. Acad. Sci. Paris* **332** (12) (2001), 1087–1092.

[20] D'Angelo, C., Papelier, Y., Mathematical modelling of the cardiovascular system and skeletal muscle interaction during exercice. In *CEMRACS 2004—mathematics and applications to biology and medicine* (ed. by Eric Cancès and J-F. Gerbeau), ESAIM Proceedings 14, EDP Sciences, Les Ulis, 2005 72–88.

[21] D'Angelo, C., Milisic, V., Reduced model for coupling of axisymmetric Navier-Stokes equations with a reaction-diffusion model for concentration. EPFL-IACS report 02.2006, submitted.

[22] Deen, W. M., Hindered transport of large molecules in liquid-filled pores. *AIChE Journal* **33** (9) (1987), 1409–1425.

[23] Deparis, S., Fernandez, M., Formaggia, L., Acceleration of a fixed point algorithm for fluid-structure interaction using transpiration conditions. *Math. Model. Numer. Anal.* **37** (4) (2003), 601–616.

[24] Deparis, S., Discacciati, M., Fourestey, G., Quarteroni, A., Fluid-structure algorithms based on Steklov-Poincaré operators. *Comput. Methods Appl. Mech. Engrg.* **195** (2006), 5797–5812.

[25] Deparis, S., Numerical Analysis of Axisymmetric Flows and Methods for Fluid-Structure Interaction Arising in Blood Flow Simulation. Ph.D. thesis, École Polytechnique Fédérale de Lausanne, 2004.

[26] Deparis, S., Gerbeau, J.-F., Vasseur, X., A dynamic preconditioner for Newton-Krylov algorithm. Application to fluid structure interaction. *INRIA, Rapport de Recherche*, No. 5277, 2004.

[27] Desjardins, B., Esteban, M. J., Existence of a weak solutions for a model of fluid-rigid structure interaction. *Arch. Ration. Mech. Anal.* **146** (1999), 59–71.

[28] Deuflhard, P., Hochmuth, R., Multiscale Analysis of Thermoregulation in the Human Microvascular System. *Math. Methods Appl. Sci.* **27** (2004), 971–989.

[29] Fernandez, M., Moubachir, M., A Newton method using exact jacobians for solving fluid-structure coupling. *Computers & Structures* **83** (2–3) (2005), 127–142.

[30] Fernandez, M., Gerbeau, J.-F., Grandmont, C., A projection semin-implicit scheme for the coupling of an eleastic structure with an incompressible fluid. *INRIA, Rapport de Recherche*, No. 5700, 2005.

[31] Fitzgibbon, G. M., Kafka, H. P., Keon, W. J., Coronary bypass fate: long-term angiographic study. *J. Amer. Coll. Cardiol.* **17** (5) (1991), 1557–1565.

[32] Formaggia, L., Gerbeau, J.-F., Nobile, F., Quarteroni, A., On the Coupling of 3D and 1D Navier-Stokes equations for Flow Problems in Compliant Vessels. *Comput. Methods Appl. Mech. Engrg.* **191** (2001), 561–582.

[33] Formaggia, L., Nobile, F., Quarteroni, A., Veneziani, A., Multiscale Modelling of the Circulatory System: a Preliminary Analysis. *Comput. Vis. Sci.* **2** (1–2) (1999), 75–83.

[34] Formaggia, L., Gerbeau, J.-F., Nobile, F., Quarteroni, A., Numerical treatment of defective boundary conditions for the Navier-Stokes equations. *SIAM J. Numer. Anal.* **40** (1) (2002), 376–401.

[35] Formaggia, L., Lamponi, D., Quarteroni, A., One dimensional models for blood flow in arteries. *J. Engrg. Math.* **47** (2003), 251–276.

[36] Formaggia, L., Quarteroni, A., Veneziani, A., The circulatory system: from case studies to mathematical modeling. In *Complex Systems in Biomedicine* (ed. by A. Quarteroni, L. Formaggia, A. Veneziani), Springer Italia, Milano 2006, 243–287.

[37] Formaggia, L., Veneziani, A., *Reduced and Multiscale Models for the Human Cardiovascular System*. Von Karman Institute Lecture Notes, Seventh Lecture Series on Biological Fluid Dynamics, 2003.

[38] Fung, Y. C., *Biomechanics: Mechanical Properties of Living Tissues*. Springer-Verlag, New York 1993.

[39] Fung, Y. C., *Biodynamics: Circulation*. Springer-Verlag, New York 1997.

[40] Galdi, G. P., Sequeira, A., Further Existence Results for Classical Solutions of the Equation of a Second Grade Fluid. *Arch. Ration. Mech. Anal.* **128** (1994), 297–312.

[41] Galdi, G. P., Rajagopal, K. R., Slow motion of a body in a fluid of second grade. *Internat. J. Engrg. Sci.* **35** (1997), 33–54.

[42] Gerbeau, J.-F., Vidrascu, M., Frey, P., Fluid-structure interaction in blood flows on geometries coming from medical imaging. *Computers & Structures* **83** (2005), 155–165.

[43] Gerbeau, J.-F, Vidrascu, M., A quasi-Newton algorithm based on a reduced model for fluid-structure interaction problems in blood flows. *Math. Model. Numer. Anal.* **37** (4) (2003), 663–680.

[44] Grandmont, C., Existence for a three-dimensional steady state fluid-structure interaction problem. *J. Math. Fluid Mech.* **4** (1) (2002), 669–694.

[45] Grandmont, C., Maday, Y., Existence for an unsteady fluid-structure interaction problem. *Math. Model. Numer. Anal.* **34** (3) (2000), 609–636.

[46] Heil, M., An efficient solver for the fully coupled solution of large displacement fluid-structure interaction problems. *Comput. Methods Appl. Mech. Engrg.* **193** (1–2) (2004), 1–23.

[47] Hochmuth, R., Deuflhard, P., Multiscale Analysis for the Bio-Heat-Transfer Equation — The Nonisolated Case. *Math. Models Methods Appl. Sci.* **14** (11) (2004), 1621–1634.

[48] Holzapfel, G. A., Gasser, T. C., Ogden, R. W., A new constitutive framework for arterial wall mechanics and a comparative study of material models. *J. Elasticity* **61** (2000), 1–48.

[49] Hoppensteadt, F., Peskin, C., *Modeling and Simulation in Medicine and the Life Sciences*. Second edition, Texts Appl. Math. 10, Springer-Verlag, New York 2002.

[50] Katchalsky, A., Curran, P. F., *Nonequilibrium Thermodynamics in Biophysics.* Harvard University Press, 1981,

[51] Kedem, O., Katchalsky, A., Thermodynamic analysis of the permeability of biological membranes to non-electrolytes. *Biochimica et Biophysica Acta* (1958), 229–246.

[52] Keener, J., Sneyd, J., *Mathematical Physiology*. Springer-Verlag, New York 1998.

[53] Lagnese, J., Leugering, G., Schmidt, E. J. P. G., *Modeling, analysis and control of dynamic elastic multi-link structures.* Systems Control Found. Appl., Birkhäuser, Boston, MA, 1994.

[54] Lamponi, D., One dimensional and Multiscale Models for Blood Flow Circulation. Ph.D. thesis, École Polytechnique Fédérale de Lausanne, 2004.

[55] Lions, J. L., Zuazua, E., Approximate controllability of a hydroelastic coupled system. *ESAIM Control Optim. Calc. Var.* **1** (1995), 1–15.

[56] Lowe, D. O., *Clinical Blood Rheology*. Vol. I, II, CRC Press, Boca Raton, Florida, 1988.

[57] Luo, X. Y., Kuang, Z. B., A study of the constitutive equation of blood. *J. Biomech.* **25** (1992), 929–934.

[58] Mallabiabarrena, I., Experimental set-up and numerical simulations of intravenous gas transfer devices. Ph.D. thesis, École Polytechnique Fédérale de Lausanne, 2003.

[59] Matthies, H., Steindorf, J., Partitioned but strongly coupled iteration schemes for nonlinear fluid-structure interaction. *Computers & Structures* **80** (2002), 1991–1999.

[60] Matthies, H., Steindorf, J., Partitioned strong coupling algorithms for fluid-structure interaction. *Computers & Structures* **81** (2003), 805–812.

[61] Matthies, H., Steindorf, J., Numerical efficiency of different partitioned methods for fluid-structure interaction. *Z. Angew. Math. Mech.* **2** (80) (2000), 557–558.

[62] Michler, C., Van Brummelen, E. H., De Borst, R., An interface Newton-Krylov solver for fluid-structure interaction. *Int. J. Numer. Methods Fluids* **47** (10-11) (2005), 1189–1195.

[63] Mok, D. P., Wall, W. A., Partitioned analysis schemes for the transient interaction of incompressible flows and nonlinear flexible structures. In *Trends in computational structural mechanics* (ed. by K. Schweizerhof, W. Wall, K. Bletzinger), International Center for Numerical Methods in Engineering (CIMNE), Barcelona 2001.

[64] Mok, D. P., Wall, W. A., Ramm, E., Accelerated iterative substructuring schemes for instationary fluid-structure interaction. In *Computational Fluid and Solid Mechanics* (ed. by K. Bathe), Elsevier, Amsterdam 2001, 1325–1328.

[65] Mouro, J., Interactions Fluide Structure en Grands Déplacements. Resolution Numerique et Application aux Composants Hydrauliques Automobiles. Ph.D. thesis, École Polytechnique, Paris 1996.

[66] Murea, C. M., Vazquez, C., Sensitivity and approximation of coupled fluid-structure equations by virtual control method. *Appl. Math. Optim.* **52** (2) (2005), 357–371.

[67] Murea, C. M., Optimal control approach for the fluid-structure interaction problems. In *Elliptic and parabolic problems* (ed. by J. Bemelmans et al.), World Scientific Publishing Co., River Edge, NJ, 2002, 442–450.

[68] Nazarov, S., Sequeira, A., Videman, J. H., Steady flows of Jeffrey-Hamel type from the half-plane into an infinite channel. Linearization on an anti-symmetric solution. *J. Math. Pures Appl.* **80** (12) (2001), 1069–1098.

[69] Nichols, W. W., O'Rourke, M. F., *Mc Donald's Blood Flow in Arteries*. Third edition, Edward Arnold Ltd., London 1990.

[70] Nobile, F., Numerical Approximation of Fluid-Structure Interaction Problems with Application to Haemodynamics. Ph.D. thesis, École Polytechnique Fédérale de Lausanne, 2001.

[71] Novotny, A., Sequeira, A., Videman, J. H., Steady motions of viscoelastic fluids in 3-D exterior domains – existence, uniqueness and asymptotic behaviour. *Arch. Ration. Mech. Anal.* **149** (1999), 49–67.

[72] Osses, A., Puel, J. P., Approximate controllability for a linear model of fluid structure interaction. *ESAIM Control Optim. Calc. Var.* **4** (1999), 497–513.

[73] Peskin, C., The immersed boundary method. *Acta Numerica* **11** (2002), 479–517.

[74] Prosi, M., Zunino, P., Perktold, K., Quarteroni, A., Mathematical and numerical models for transfer of low density lipoproteins through the arterial walls: a new methodology for the model set up with applications to the study of disturbed lumenal flow. *J. Biomech.* **38** (2005), 903–917.

[75] Quarteroni, A., Formaggia, L., Mathematical Modelling and Numerical Simulation of the Cardiovascular System. In *Modelling of Living Systems* (ed. by P. G. Ciarlet and J. L. Lions), Handbook of Numerical Analysis Series 12, Elsevier, Amsterdam 2004, 3–127.

[76] Quarteroni, A., Rozza, G., Optimal control and shape optimization in aorto-coronaric bypass anastomoses. *Math. Models Methods Appl. Sci.* **13** (12) (2003), 1801–1823.

[77] Quarteroni, A., Valli, A., *Numerical Approximation of Partial Differential Equations*. Springer Ser. Comput. Math. 23, Springer-Verlag, Berlin 1994.

[78] Quarteroni, A., Valli, A., *Domain Decomposition Methods for Partial Differential Equations*. Oxford University Press, New York 1999.

[79] Quarteroni, A., Veneziani, A., Zunino, P., Mathematical and numerical modelling of solute dynamics in blood flow and arterial walls. *SIAM J. Numer. Anal.* **39** (5) (2002), 1488–1511.

[80] Quarteroni, A., Veneziani, A., Zunino, P., A Domain Decomposition Method for Advection-Diffusion Processes with Application to Blood Solutes. *SIAM J. Sci. Comput.* **23** (6) (2002), 1959–1980.

[81] Quarteroni, A., Veneziani, A., Analysis of a geometrical multiscale model based on the coupling of ODEs and PDEs for blood flow simulations. *SIAM Mult. Models Sim.* **1** (2) (2003), 173–195.

[82] Raback, P., Ruokolainen, J., Lyly, M., Järvinen. Fluid-structure interaction boundary conditions by artificial compressibility. In ECCOMAS *Computational Fluid Dynamics Conference*, Swansea, 2001.

[83] Rajagopal, K. R., Bhatnagar, R. K., Flow of an Oldroyd-B fluid due to a stretching sheet in the presence of a free stream velocity. *Internat. J. Non-Linear Mech.* **30** (3) (1995), 391–405.

[84] Robertson, A. M., Sequeira, A., A director theory approach for modeling blood flow in te arterial system: an alternative to classical 1d models. *Math. Models Methods Appl. Sci.* **15** (6) (2005), 871–906.

[85] Rozza, G., Shape Design by Optimal Flow Control and Reduced Basis Techniques: Applications to Bypass Configurations in Haemodynamics. Ph.D. thesis, École Polytéchnique Fédérale de Lausanne, 2005.

[86] Serrin, J., Mathematical principles of classical fluid mechanics. In *Handbuch der Physik* (ed. by S. Flügge and C. Truesdell), Vol. VIII/1, Springer-Verlag, Berlin 1959, 125–263.

[87] Smith, N. P., Nickerson, D. P., Crampin, E. J., Hunter, P. J., Multiscale computational modelling of the heart. *Acta Numer.* **13** (2004), 371–431.

[88] Tallec, P. L., Mouro, J., Fluid structure interaction with large structural displacements. *Comput. Methods Appl. Mech. Engrg.* **190** (2001), 3039–3067.

[89] Jo, H., Dull, R. O., Hollis, T. M., Tarbell, J. M., Endothelial albumin permeability is shear dependent, time dependent and reversible. *Amer. J. Physiol.* **260** (1991), H1992–H1996.

[90] Wang D. M., Tarbell, J. M., Modelling interstitial flow through arterial media. *ASME J. Biomech. Eng.* **117** (1995), 358–363.

[91] Tarbell, J. M., Lever, M. J., Caro, C. G., The effect of varying albumin concentration and hydrostatic pressure on hydraulic conductivity of the Rabbit common carotid artery. *Microvasc. Res.* **35** (1988), 204–220.

[92] Taylor, C. A., Draney, M. T., Ku, J. P., Parker, D., Steele, B. N., Wang, K., Zarins, C. K., Predictive medicine: Computational techniques in therapeutic decision-making. *Computer Aided Surgery* **4** (5) (1999), 231–247.

[93] Tezduyar, T., Finite element methods for fluid dynamics with moving boundaries and interfaces. *Arch. Comput. Methods Engrg.* **8** (2001), 83–130.

[94] Thurston, G. B., Viscoelstic properties of blood and blood analogs. *Avances in Hemodynamics and hemorheology* **1** (1996), 1–30.

[95] Truskey, G. A., Roberts, W. L., Herrmann, R. A., Malinauskas, R. A., Measurement of endothelial permeability to I-low density lipoproteins in rabbit arteries by use of en face preparations. *Circ. Res.* **7** (4) (1992), 883–897.

[96] Varty, K., Allen, K. E., Bell, P. R. F., London, N. J. M., Infra-inguinal vein graft stenosis. *Br. J. Surg.* **80** (1993), 825–833.

[97] Veneziani, A., Vergara, C., Flow rate defective boundary conditions in haemodynamics simulations. *Int. J. Numer. Methods Fluids* **47** (2005), 803–816.

[98] Veneziani, A., Vergara, C., An approximate method for solving incompressible Navier–Stokes problems with flow rate conditions. *MOX report* **70**, Department of Mathematics, Politecnico di Milano, 2005.

[99] Wada, S., Karino, T., Computational study on LDL transfer from flowing blood to arterial walls. In *Clinical Application of Computational Mechanics to the Cardiovascular System* (ed. by T. Yamaguchi), Springer-Verlag, 2000.

[100] Wang, J. J., Parker, K. H., Wave propagation in a model of the arterial circulation. *J. Biomech.* **37** (2004), 457–470.

[101] Womersley J. R., Method for the calculation of velocity, rate of flow and viscous drag in arteries when the pressure gradient is known. *J. Physiol.* **127** (1955), 553–563.

[102] Yeleswarapu, K. K, Evaluation of Continuum Models for Characterizing the Constitutive Behavior of Blood. Ph.D. thesis, Department of Mechanical Engineering, University of Pittsburgh, 1996.

[103] Zhang, X., Zuazua, E., Polynomial decay and control of a 1-d hyperbolic-parabolic coupled system. *J. Differential Equations* **204** (2) (2004), 380–438.

[104] Zhang, X., Zuazua, E., Long time behavior of a coupled heat-wave system arising in fluid-structure interaction. *Arch. Ration. Mech. Anal.* **184** (2007), 49–120.

[105] Zunino, P., Mathematical and numerical modeling of mass transfer in the vascular system. Ph.D. thesis, École Polytechnique Fédérale de Lausanne, 2002.

[106] Zunino, P., Multidimensional pharmacokinetic models applied to the design of drug eluting stents. *Cardiov Eng.* **4** (2) (2004), 181–191.

[107] Zunino, P., Mastalli, D., Quarteroni, A., VanBiesen, W., Vecten, D., Pacitti, A., Lameire, N., Neftel, F., Wauters, J. P., Development of a new mathematical approach to optimize peritoneal dialysis. EPFL-IACS report 03.2006.

Modelling and Scientific Computing (CMCS), Institute of Analysis and Scientific Computing (IACS), EPFL, École Polytechnique Fédérale de Lausanne, 1015, Lausanne, Switzerland

and

Dipartimento di Matematica "Francesco Brioschi", MOX, Modellistica e Calcolo Scientifico, Politecnico di Milano, 20133 Milano, Italy

E-mail: alfio.quarteroni@epfl.ch